8. Zhao Y, Yin X, Qin H, *et al*: Two supporting factors greatly improve the efficiency of human iPSC generation. Cell Stem Cell 3: 475-479, 2008.
9. Kawamura T, Suzuki J, Wang YV, *et al*: Linking the p53 tumour suppressor pathway to somatic cell reprogramming. Nature 460: 1140-1144, 2009.
10. Hong H, Takahashi K, Ichisaka T, *et al*: Suppression of induced pluripotent stem cell generation by the p53-p21 pathway. Nature 460: 1132-1135, 2009.
11. Nagai K, Ishii H, Miyoshi N, *et al*: Long-term culture following ES-like gene-induced reprogramming elicits an aggressive phenotype in mutated cholangiocellular carcinoma cells. Biochem Biophys Res Commun 395: 258-263, 2010.
12. Feldmann G, Beaty R, Hruban RH and Maitra A: Molecular genetics of pancreatic intraepithelial neoplasia. J Hepatobiliary Pancreat Surg 14: 224-232, 2007.
13. Prenen H, Tejpar S and Van Cutsem E: New strategies for treatment of KRAS mutant metastatic colorectal cancer. Clin Cancer Res 16: 2921-2926, 2010.
14. Laurent-Puig P and Zucman Rossi J: Genetics of hepatocellular tumors. Oncogene 25: 3778-3786, 2006.
15. Tannapfel A, Sommerer F, Benicke M, *et al*: Mutations of the BRAF gene in cholangiocarcinoma but not in hepatocellular carcinoma. Gut 52: 706-712, 2003.
16. Ray KC, Bell KM, Yan J, Gu G, Chung CH, Washington MK and Means AL: Epithelial tissues have varying degrees of susceptibility to Kras(G12D)-initiated tumorigenesis in a mouse model. PLoS One 6: e16786, 2011.

OPEN ACCESS Freely available online

PLOS ONE

A Versatile Technique for the *In Vivo* Imaging of Human Tumor Xenografts Using Near-Infrared Fluorochrome-Conjugated Macromolecule Probes

Hiroshi Suemizu[1]*, Kenji Kawai[2], Yuichiro Higuchi[1], Haruo Hashimoto[1], Tomoyuki Ogura[3], Toshio Itoh[4], Erika Sasaki[5], Masato Nakamura[2,6]

1 Biomedical Research Department, Central Institute for Experimental Animals, Kawasaki, Japan, **2** Pathology Research Department, Central Institute for Experimental Animals, Kawasaki, Japan, **3** Animals Resource Department, Central Institute for Experimental Animals, Kawasaki, Japan, **4** Marmoset Research Department, Central Institute for Experimental Animals, Kawasaki, Japan, **5** Department of Applied Developmental Biology, Central Institute for Experimental Animals, Kawasaki, Japan, **6** Department of Pathology and Regenerative Medicine, Tokai University School of Medicine, Isehara, Japan

Abstract

Here, we present a versatile method for detecting human tumor xenografts *in vivo*, based on the enhanced permeability and retention (EPR) effect, using near-infrared (NIR) fluorochrome-conjugated macromolecule probes. Bovine serum albumin (BSA) and two immunoglobulins—an anti-human leukocyte antigen (HLA) monoclonal antibody and isotype control IgG_{2a}—were labeled with XenoLight CF770 fluorochrome and used as NIR-conjugated macromolecule probes to study whole-body imaging in a variety of xenotransplantation mouse models. NIR fluorescent signals were observed in subcutaneously transplanted BxPC-3 (human pancreatic cancer) cells and HCT 116 (colorectal cancer) cells within 24 h of NIR-macromolecule probe injection, but the signal from the fluorochrome itself or from the NIR-conjugated small molecule (glycine) injection was not observed. The accuracy of tumor targeting was confirmed by the localization of the NIR-conjugated immunoglobulin within the T-HCT 116 xenograft (in which the orange-red fluorescent protein tdTomato was stably expressed by HCT 116 cells) in the subcutaneous transplantation model. However, there was no significant difference in the NIR signal intensity of the region of interest between the anti-HLA antibody group and the isotype control group in the subcutaneous transplantation model. Therefore, the antibody accumulation within the tumor *in vivo* is based on the EPR effect. The liver metastasis generated by an intrasplenic injection of T-HCT 116 cells was clearly visualized by the NIR-conjugated anti-HLA probe but not by the orange-red fluorescent signal derived from the tdTomato reporter. This result demonstrated the superiority of the NIR probes over the tdTomato reporter protein at enhancing tissue penetration. In another xenograft model, patient-derived xenografts (PDX) of LC11-JCK (human non-small cell lung cancer) were successfully visualized using the NIR-conjugated macromolecule probe without any genetic modification. These results suggested that NIR-conjugated macromolecule, preferably, anti-HLA antibody probe is a valuable tool for the detection of human tumors in experimental metastasis models using whole-body imaging.

Citation: Suemizu H, Kawai K, Higuchi Y, Hashimoto H, Ogura T, et al. (2013) A Versatile Technique for the *In Vivo* Imaging of Human Tumor Xenografts Using Near-Infrared Fluorochrome-Conjugated Macromolecule Probes. PLoS ONE 8(12): e82708. doi:10.1371/journal.pone.0082708

Editor: Joseph Najbauer, University of Pécs Medical School, Hungary

Received April 1, 2013; **Accepted** October 26, 2013; **Published** December 17, 2013

Copyright: © 2013 Suemizu et al. This is an open-access article distributed under the terms of the Creative Commons Attribution License, which permits unrestricted use, distribution, and reproduction in any medium, provided the original author and source are credited.

Funding: A part of this work was supported by a Grant-in-Aid for Scientific Research (21240042) to HS from the Ministry of Education, Culture, Sports, Science, and Technology (MEXT) of Japan: the Project for the Realization of Regenerative Medicine from MEXT of Japan. The funders had no role in study design, data collection and analysis, decision to publish, or preparation of the manuscript.

Competing Interests: The authors have declared that no competing interests exist.

* E-mail: suemizu@ciea.or.jp

Introduction

Human tumor xenograft (subcutaneous) models have been very popular *in vivo* models in oncology research. However, these models may not adequately reflect the pathophysiological environments in which cancer cells exist [1]. Liver metastasis xenograft models in relevant orthotopic locations, such as colorectal tumors metastasized to the liver, have been developed by intrasplenic (*isp*) injection of tumor cells into immunodeficient mice [2]. We have previously developed a reliable model system for assaying hematogenous liver metastases of pancreatic and colorectal cancers in NOG mice [3,4]. The efficacy of farnesyl transferase inhibitors (FTIs) against HCT 116 (colorectal cancer) cells was evaluated in this model, and the effectiveness of this treatment was demonstrated by the prolonged survival times of mice treated with FTIs [4]. In most cases, treatment effectiveness is assessed in terms of survival or gross findings in the liver, as animal sacrifice is usually required. Therefore, novel and less invasive approaches for preclinical studies are required to evaluate the effectiveness of anti-tumor drugs *in vivo*.

In particular, optical bioimaging without radioactive tracers or ionizing radiation is suitable for such preclinical studies and facilitates serial measurements of xenografts, even when located intraperitoneally or in other orthotopic locations [5]. However, optical probes labeled with fluorochromes that emit light in the 400—700 nm range, such as green fluorescent protein (GFP), have limited tissue penetration and high tissue autofluorescence [6]. Hence, fluorescent proteins (FPs) that have much longer wavelengths than GFP have been developed; these proteins fluoresce as orange-red and far-red, avoiding absorption by hemoglobin at

wavelengths below 600 nm [7,8]. The major bottleneck in most bioimaging experiments using fluoroproteins is the requirement to have previously transfected the corresponding gene into the target cells.

It is known that macromolecules such as albumin, transferrin, immunoglobulin, and α2-macroglobulin accumulate in solid tumors through the enhanced permeability and retention (EPR) effect caused by leaky vasculature within the tumor [9,10]. This effect can facilitate binding between receptors and ligands, such as antibodies and adhesion molecules. Recently, Keereweer et al. reported the detection of oral cancer in an orthotopic mouse model using near-infrared (NIR) fluorescence agents that targeted either the αvβ3 integrins or the EPR effect [11]. In mice xenograft models, human and mouse cells display different major histocompatibility complex (MHC) surface antigens [12]. Therefore, these antigens are good target molecules for distinguishing between human cells and recipient mouse cells in xenograft tissue sections [13,14]. Because of this, antibodies against the MHC class I antigens (HLA-A, -B, and -C in humans) such as the anti-HLA-ABC antibody, have been used as "Xenograft markers" for the detection of human cells by flow cytometry, immunoblotting, and immunohistochemical staining. Currently, there are no reports describing the use of this anti-HLA antibody as an *in vivo* imaging probe. Therefore, we sought to develop a versatile method using anti-HLA antibody for the detection of human tumors *in vivo* without the need for fluoroprotein expression. The anti-HLA-ABC antibody was conjugated with molecules that fluoresce in the NIR optical spectrum (650–900 nm), reducing background fluorescence and enhancing tissue penetration compared with fluorescent probes of shorter wavelengths. We assessed the feasibility of tumor detection in various xenotransplantation models using an NIR-conjugated anti-HLA antibody that targeted either the EPR effect or antigen–antibody binding. We showed that the NIR-probe was superior to the tdTomato reporter protein at enhancing tissue penetration *in vivo*. These results suggested that NIR-conjugated anti-HLA antibody probe is a valuable tool for the detection of human tumor xenografts in experimental mouse models using whole-body optical imaging.

Materials and Methods

Cell Culture

The human colorectal cancer cell line HCT 116 and the human pancreatic cancer cell line BxPC-3 were obtained from the American Type Culture Collection (Manassas, VA, USA) and were maintained in McCoy's 5A and RPMI-1640 medium (Sigma, St. Louis, MO, USA), respectively, supplemented with antibiotics and 10% fetal bovine serum. Cells were incubated in a humidified incubator (37°C, 5% CO_2) and were passaged upon reaching 80% confluence. To establish HCT 116 cell expressing the orange-red fluorescent protein tdTomato (Abs/Em = 554/581 nm) (T-HCT 116) as a control for fluoroimaging, HCT 116 cells were transfected with the ptdTomato-N1 vector (Clontech Laboratories, Inc. Mountain View, CA, USA) using magnetofection (Oz Biosciences, France) according to the manufacturer's instructions. Two days after transfection, 500 μg/ml of neomycin (Invitrogen Corp., Carlsbad, CA) was added, and the cultures were maintained until cell death ceased.

NIR fluorescent agents

For the direct detection of human tumors *in vivo*, the near-infrared (NIR)-conjugated anti-HLA antibody (NIR-αHLA) was prepared as follows. The mouse monoclonal anti-human HLA-ABC antibody clone W6/32 (IgG_{2a}; Cedarlane Laboratories USA Inc., Burlington, NC, USA) and an isotype-matched mouse IgG_{2a} antibody (SouthernBiotech, Birmingham, AL, USA) were conjugated to the IVIS XenoLight^{TM} CF770 (Abs/Em = 770/797 nm) fluorochrome using the Fluorescent Dye kit for *In Vivo* Imaging (Caliper Life Sciences, Hopkinton, MA, USA) according to the manufacturer's instructions. The absorbance of the NIR-conjugated antibodies was measured at 280 and 770 nm using a SmartSpec^{TM} 3000 spectrophotometer (BioRad Laboratories, Hercules, CA, USA). The final concentration of the antibody conjugate and the degree of labeling (DOL) were calculated using the following formulae:

$$[Conjugate](mg/mL) = \{[A_{280} - (A_{770} \times CF)]/1.4\} \times dilutionfactor;$$

CF is the absorbance correction factor (0.06 for XenoLight CF770), and the value 1.4 is the extinction coefficient of whole (H+L) IgG.

$$[DOL](dye/protein) = (A_{770} \times Mwt \times dilutionfactor)/(\varepsilon \times [Conjugate])$$

Mwt is the molecular weight (150,000 for IgG), and ε is the molar extinction coefficient (220,000 for XenoLight CF770). Bovine serum albumin (BSA; Nacalai, Kyoto, Japan) was also conjugated to the XenoLight^{TM} CF770 fluorochrome (NIR-BSA), and the DOL was calculated using the extinction coefficient (0.66) and Mwt (67,000) of BSA. The DOL in the NIR-αHLA (0.89 mg protein/mL), the NIR-conjugated mouse isotype control IgG_{2a} immunoglobulin (NIR-Isotype; 0.60 mg protein/mL), and BSA (0.73 mg protein/mL) were 1.34, 1.42, and 0.72 dye/protein, respectively. Free fluorochrome (Free NIR) and fluorochrome-glycine (NIR-Glycine), which is produced when the conjugation procedure is quenched by the addition of excess glycine (Nacalai, Kyoto, Japan), were used as negative control probes.

Animals

All mice studies were conducted in strict accordance with the Guide for the Care and Use of Laboratory Animals from the Central Institute for Experimental Animals. All experimental protocols were approved by the Animal Care Committee of the CIEA (Permit Number: 11029A). All surgeries were performed under isoflurane anesthesia, and all efforts were made to minimize animal suffering. For whole-body optical imaging, we established an immunodeficient hairless mouse strain, the BALB/cA *Rag2*^{null} *Il2rg*^{null} *nude* (C.Cg-*Rag2*^{tm1} *Il2rg*^{tm1Sug} *Foxn1*^{nu}/Jic; abridged name: BRG nude) strain. This strain was created by crossing the BALB/cA *Rag2*^{null} *Il2rg*^{null} (C.Cg-*Rag2*^{tm1} *Il2rg*^{tm1Sug}/Jic; abridged name: BRG) strain [15] and the BALB/cA *nude* (C.Cg-*Foxn1*^{nu}/Jic; abridged name: nude) strain [16]. To produce an orthotopic pancreatic cancer model, immunodeficient NOG (NOD.Cg-*Prkdc*^{scid} *Il2rg*^{tm1Sug}/ShiJic) mice were used as transplantation hosts [17].

Xenograft Models

To generate xenograft models and liver and hematogenous metastasis models, 1×10^5 HCT 116 and T-HCT 116 cells were suspended in 0.1 mL of serum-free medium and then subcutane-

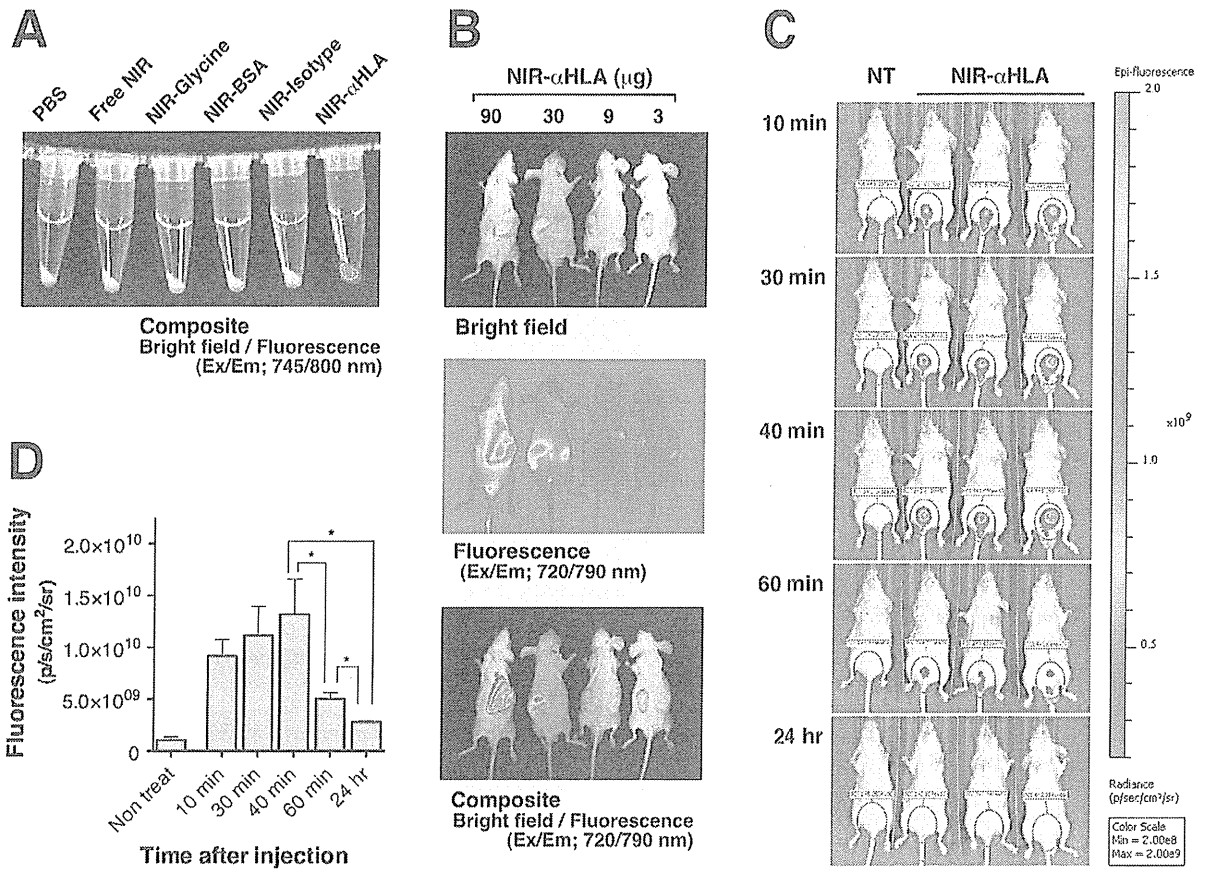

Figure 1. Reactivity of the NIR-αHLA probe with HCT 116 (human colorectal cancer) cells *in vitro* and *in vivo*. (A) HCT 116 cells were incubated with various NIR-probes, and the *in vitro* fluorescence signals were specifically detected at wavelengths of 745/800 nm, which were overlaid onto a bright-field image. (B) *In vivo* fluorescence images of HCT 116 tumor-bearing BRG nude mice. Dose-related effects of the NIR fluorescence intensities after *iv* injection of various amounts of NIR-αHLA probe can been observed. Fluorescent signal from the NIR-αHLA probe was specifically detected at wavelengths of 720/790 nm. The bright-field image is shown in the top panel, the fluorescent image is shown in the middle panel, and the overlay image is shown in the bottom panel. (C) The time course of the NIR fluorescence intensity of BRG nude mice that had received an *iv* injection of the NIR-αHLA probe. (D) Fluorescence intensities were quantified using ROIs of equivalent-sized areas from the lower abdominal regions at the indicated time points. Data are presented as the mean ± SD of three individual mice (Student's *t* test, **p* value of 40 min and 60 min = 0.0390, for 40 min and 24 hr = 0.0151, and for 60 min and 24 hr = 0.0313).
doi:10.1371/journal.pone.0082708.g001

ously (*sc*) transplanted into the left flank of 7–9 week-old BRG nude mice (n = 10 and 8, respectively). To generate tumor xenografts in both the subcutaneous spaces of 7–9 week-old BRG nude mice (n = 5), 1×10^6 HCT 116 and BxPC-3 cells were suspended in 0.1 mL of serum free medium and were *sc* transplanted into the left and right flank, respectively. Liver metastases of human colorectal cancer cells were generated by intrasplenic (*isp*) injections of 1×10^5 T-HCT 116 cells and 1×10^6 HCT 116 cells into BRG nude mice (n = 3 and 3, respectively), followed by splenectomy under isoflurane anesthesia [4]. Hematogenous metastases of HCT 116 cells were generated by an intravenous (*iv*) injection of 1×10^5 cells into BRG nude mice (n = 3). To generate an orthotopic implantation model of pancreatic cancer, BxPC-3 cells (1×10^6 cells/head) were injected intrasplenically (*isp*) into splenic vein-ligated 9 week-old NOG mice, and a splenectomy was then performed (n = 2). Human non-small cell lung cancer (NSCLC) xenografts [18] were created by the *sc* implantation of LC11-JCK cells by trocar cannula into the left flank of BRG nude mice (n = 4).

In vivo animal imaging

Spectral fluorescence images were obtained using the Kodak *In Vivo* Imaging System FX (Carestream Health, Inc. Rochester, NY, USA) and the IVIS SpectrumCT (Caliper Life Sciences, Hopkinton, MA, USA). After an intravenous injection with 100 μL of the NIR fluorochrome-conjugated probes, whole-body fluorescence images were obtained under isoflurane anesthesia. The NIR-conjugated macromolecule probes (including NIR-BSA, NIR-Isotype, and NIR-αHLA) were detected at wavelengths of 720 nm (excitation) and 790 nm (emission); the tdTomato fluoroprotein was detected at an excitation wavelength of 535 nm and an emission wavelength of 600 nm using the Kodak *In-Vivo* Imaging System FX. The NIR fluorescent signal was detected at a 745 nm excitation wavelength and an 800 nm emission wavelength using the IVIS SpectrumCT. Bright-field photographs were obtained for each imaging time. The merged bright-field photographs and fluorescence images were generated using the Kodak Molecular Imaging software SE5.0 (Carestream Health, Inc.) and the Living Image software 4.1.3 (Caliper Life Sciences).

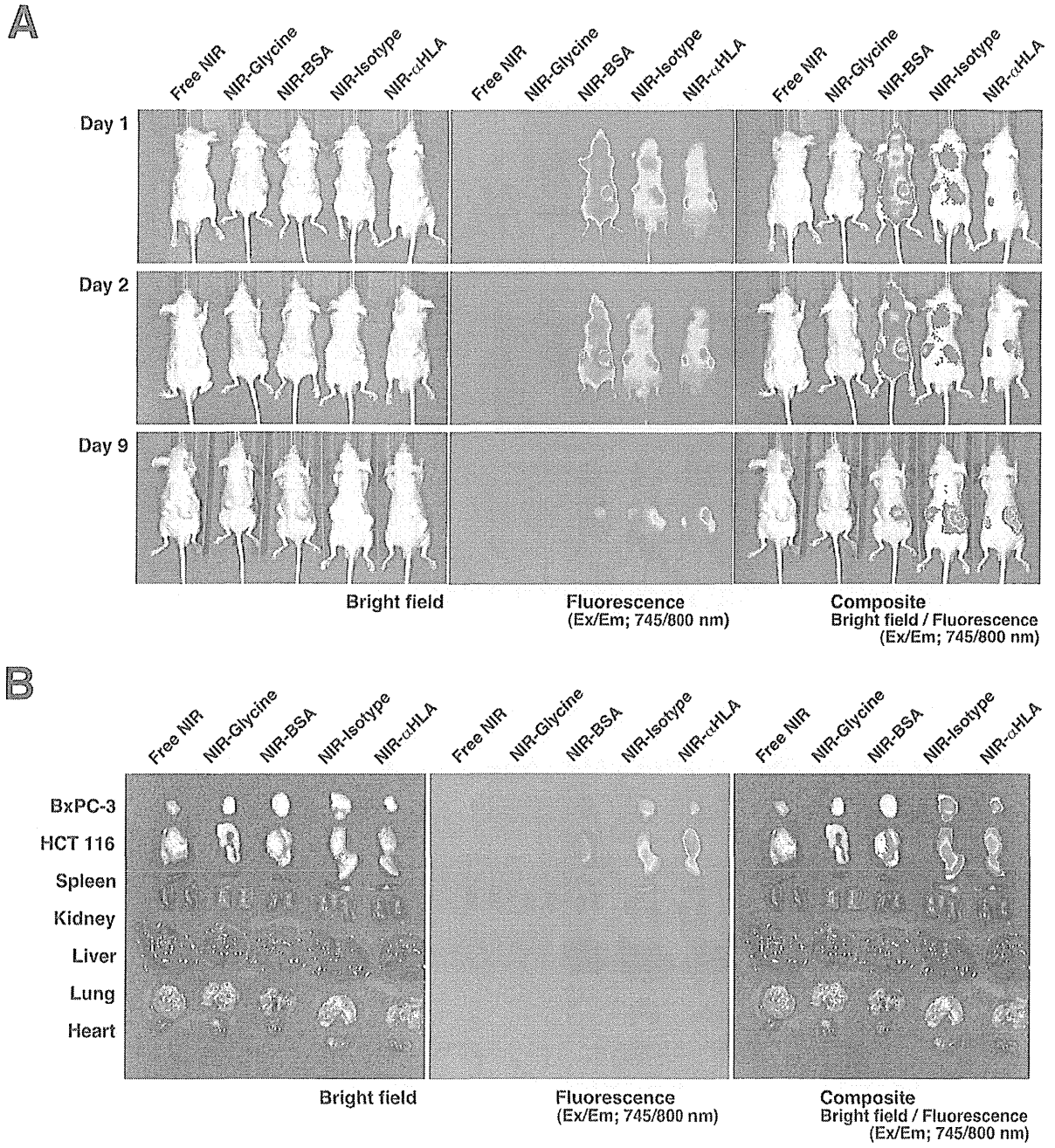

Figure 2. Proof of concept experiments for the *in vivo* imaging of human tumors with the NIR-probes. (A) *In vivo* fluorescence images of BxPC-3 and HCT 116 tumor-bearing BRG nude mice (left and right flank, respectively) were taken 1, 2, and 9 days after *iv* injections with various NIR-probes. (B) *Ex vivo* fluorescence images of the BxPC-3 and HCT 116 xenografts and tissues of recipient BRG nude mice. The bright-field photograph is shown in the left panel, the fluorescence image is shown in the center panel, and the overlay image is shown in the right panel. The fluorescent signal from the NIR-probes were specifically detected at 745/800 nm using an IVIS SpectrumCT.
doi:10.1371/journal.pone.0082708.g002

Fluorescent intensity was quantified in the region of interest (ROI). Identical illumination settings (lamp voltage, filters, f/stop, field of views, binning) were used for acquiring all images, and the fluorescence emission was normalized to photons per second per centimeter square per steradian (p/s/cm^2/sr) in the quantitative analysis. All NIR fluorescent images were acquired using 1 second-exposure time (f/stop = 2) and displayed in the same scale of fluorescent intensity. Mice were sacrificed by exsanguination under isoflurane anesthesia immediately after the completion of the imaging. Abdominal surgery was then conducted to clearly show the cancer cell engraftments and to enable *in situ* and *ex vivo* optical imaging using the same system.

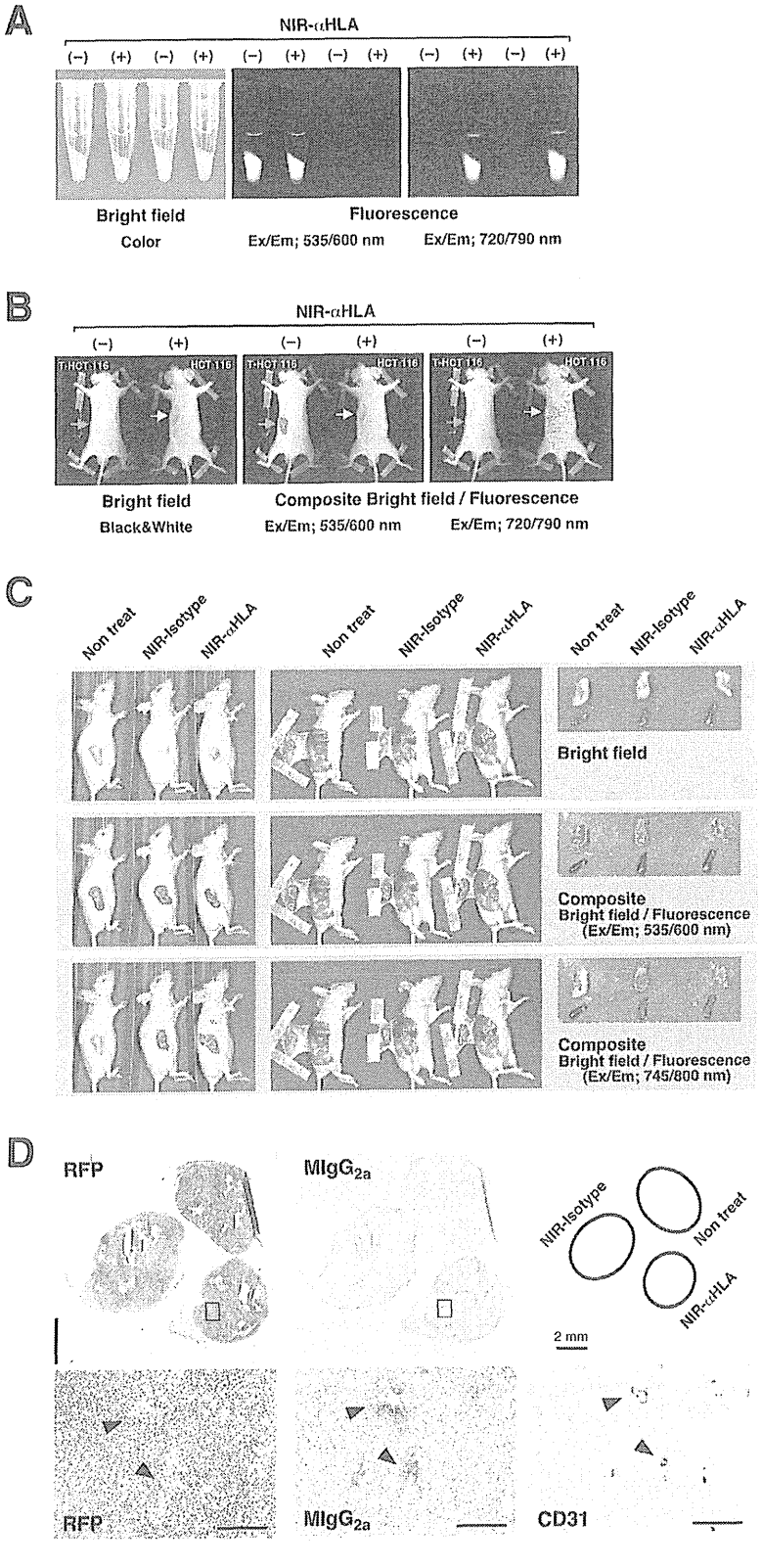
A
NIR-αHLA
(−) (+) (−) (+) (−) (+) (−) (+) (−) (+) (−) (+)
Bright field
Color
Fluorescence
Ex/Em; 535/600 nm
Ex/Em; 720/790 nm
B
NIR-αHLA
(−) (+) (−) (+) (−) (+)
Bright field
Black&White
Composite Bright field / Fluorescence
Ex/Em; 535/600 nm
Ex/Em; 720/790 nm
C
Non treat
NIR-Isotype
NIR-αHLA
Bright field
Composite
Bright field / Fluorescence
(Ex/Em; 535/600 nm)
Composite
Bright field / Fluorescence
(Ex/Em; 745/800 nm)
D
RFP
MIgG2a
NIR-Isotype
Non treat
NIR-αHLA
2 mm
RFP
MIgG2a
CD31

Figure 3. Validation of *in vivo* imaging of human tumors with the NIR-conjugated macromolecule probes. (A) Bright-field images and fluorescence images of the T-HCT 116 cells (which express tdTomato) and HCT 116 cells *in vitro*. Fluorescent signal from the orange-red fluorescent protein tdTomato and the NIR-αHLA probe were specifically detected at wavelengths of 535/600 nm and 720/790 nm, respectively. The absence or presence of the NIR-αHLA antibody is indicated as NIR-αHLA (-) or (+), respectively. (B) *In vivo* fluorescence images of T-HCT 116 and HCT 116 tumor-bearing BRG nude mice. The NIR fluorescence intensity 2 days after *iv* injection of the NIR-αHLA probe can be observed. Fluorescent signal from tdTomato and NIR-αHLA probe were specifically detected at wavelengths of 535/600 nm and 720/790 nm, respectively, using the Kodak *In-Vivo* Imaging System FX. The absence or presence of the NIR-αHLA probe is indicated as NIR-αHLA (-) or (+), respectively. The red and yellow arrows indicate engraftment sites of T-HCT 116 cells and HCT 116 cells, respectively. (C) Fluorescent signal of the NIR-conjugated macromolecule probes co-localized with tdTomato in T-HCT 116 cells in tumor-bearing BRG mice. The fluorescent signals at 535/600 nm and 745/800 nm were overlaid (composite) using Living Image software 4.1.3. Li; liver, Sp; spleen. (D) Immunohistochemical staining of dissected tumors; anti-RFP (RFP; left), anti-mouse IgG_{2a} ($MIgG_{2a}$; center), and anti-CD31 (CD31; right); Enlarged view of boxed area shown below. Arrowheads indicate same position the on serial section. Scale bar, 200 μm.
doi:10.1371/journal.pone.0082708.g003

Immunohistochemical staining

Mice were euthanized by exsanguination under anesthesia, and xenograft tumors were excised and embedded in OCT compound (Sakura Finetek Japan Co., Ltd., Tokyo, Japan) and frozen in liquid nitrogen. Five-micron-thick serial frozen sections were prepared and fixed with 4% (v/v) paraformaldehyde (Wako Pure Chemical Industries, Ltd., Osaka, Japan). Nonspecific peroxidase activity was quenched by incubation with 0.3% hydrogen peroxide for 5 min. Sections were incubated primarily with rabbit polyclonal anti-red fluorescent protein (RFP; Abcam, Cambridge, UK), goat polyclonal mouse anti-IgG_{2a} (Bethyl Laboratories, Montgomery, TX, USA) antibodies, and rat monoclonal mouse anti-CD31 (PECAM-1) (Dianova, Hamburg, Germany) antibodies for overnight at 4°C. Signals were detected using a immune-enzyme polymer method (Nichirei, Tokyo, Japan) using a 3,3′-diaminobenzidine tetrahydrochloride (DAB; Dojindo Laboratories, Kumamoto, Japan) substrate as a chromogen. Sections were counterstained with hematoxylin.

Statistical Analyses

Statistical analyses were performed with the Prism 5 software (GraphPad Software, CA, USA).

Results

Confirmation of NIR-αHLA specificity for human cancer cells

To confirm the specificity of the fluorochrome-conjugated probes *in vitro*, HCT 116 (human colorectal cancer) cells were treated with Free NIR, NIR-Glycine, NIR-BSA, NIR-Isotype (isotype control), or NIR-αHLA. Fluorescence imaging of the NIR-probes was then conducted using the excitation/emission 745/800 nm filter sets. Only the cells treated with NIR-αHLA fluoresced, and fluorescence were not observed in the cells treated with the other NIR-probes (Figure 1A).

To assess whether the NIR-αHLA probe could be used to visualize human tumors *in vivo*, BRG nude mice were *sc* transplanted with HCT 116 cells and were imaged after *iv* injection with different amounts of the NIR-αHLA probe. The mice were injected with the NIR-αHLA probe (90, 30, 9, or 3 μg/mouse) and were imaged on day 1 (Figure 1B). The NIR signal was observed in the tumor regions of the mice that had received an injection of more than 30 μg NIR-αHLA probe. The rapid clearance of the NIR-αHLA probe was confirmed by fluorescence imaging (Figure 1C). The accumulation of fluorescence in the bladder peaked at 40 min, and the NIR fluorescence disappeared within 24 hr after NIR-αHLA probe injection (Figure 1D).

Specificity of NIR-conjugated macromolecule probe accumulation in tumor xenografts

As seen in an *in vitro* study of HCT 116 cells, fluorescence was observed in BxPC-3 (human pancreatic cancer) cells *in vitro* only when the cells were treated with the NIR-αHLA probe (data not shown). To validate the NIR-αHLA probe specificity for tumor cells *in vivo*, BRG nude mice were *sc* transplanted with BxPC-3 cells and HCT 116 cells on the left and right flanks, respectively, and were imaged after *iv* injection of the different NIR-probes with equivalent amounts of fluorochrome. The mice were imaged on days 1, 2, and 9 after NIR-probe injection (Figure 2A). On day 1 after probe injection, the mice injected with NIR-BSA, NIR-Isotype, or the NIR-αHLA probe accumulated fluorescent signals in the tumor regions. However, the mice injected with the small molecular probes (Free NIR and NIR-Glycine) did not show any fluorescent signal accumulation. These results implied that the NIR-conjugated macromolecules (BSA and immunoglobulin (IgG)) accumulated in the tumors mainly as a result of the EPR effect. Nine days after NIR-probe injection, the fluorescent signals in the tumor regions were decreased in the mice that had been injected with NIR-BSA and NIR-Isotype; overall, a decrease in background fluorescence was also observed. In contrast, the fluorescence signals derived from the NIR-αHLA probe seemed to be retained in the tumor region despite the disappearance of the background fluorescence. This specificity and prolonged retention of the NIR-αHLA probe coincided with the *ex vivo* imaging (Figure 2B). The strongest NIR signals were observed in the tumors excised from mice that had been injected with the NIR-αHLA probe.

To confirm the specificity of the NIR-conjugated macromolecule probe *in vitro*, orange-red fluorescent protein tdTomato-expressing HCT 116 cells (T-HCT 116 cells) and HCT 116 cells were treated with the NIR-αHLA probe (Figure 3A). Fluorescence imaging of tdTomato and the NIR-αHLA probe was then conducted using the excitation/emission filter sets of 535/600 and 720/790 nm, respectively. The cells treated with the NIR-αHLA probe showed fluorescent signals with the 720/790 nm filter set; however, the fluorescent signals were not observed in the cells in the absence of the NIR-αHLA probe. Fluorescence of the accumulated tdTomato protein was detected only in T-HCT 116 cells, using the 535/600 nm filter set. When transplanted cancer cells became visible and palpable, the mice were injected with the NIR-αHLA probe (90 μg/mouse). The mice were imaged 2 days after NIR-αHLA probe injection (Figure 3B). Fluorescence of the NIR signal was observed in the tumor regions within 1 day of probe injection, was optimal at 2 days, and remained visible for up to 14 days after antibody injection (data not shown). The T-HCT 116 cells were used as a fluorescence imaging control. Fluorescence of the accumulated tdTomato protein was detected using the 535/600 nm filter set, but the fluorescent signals were not detected with the 720/790 nm filter set. These results indicated

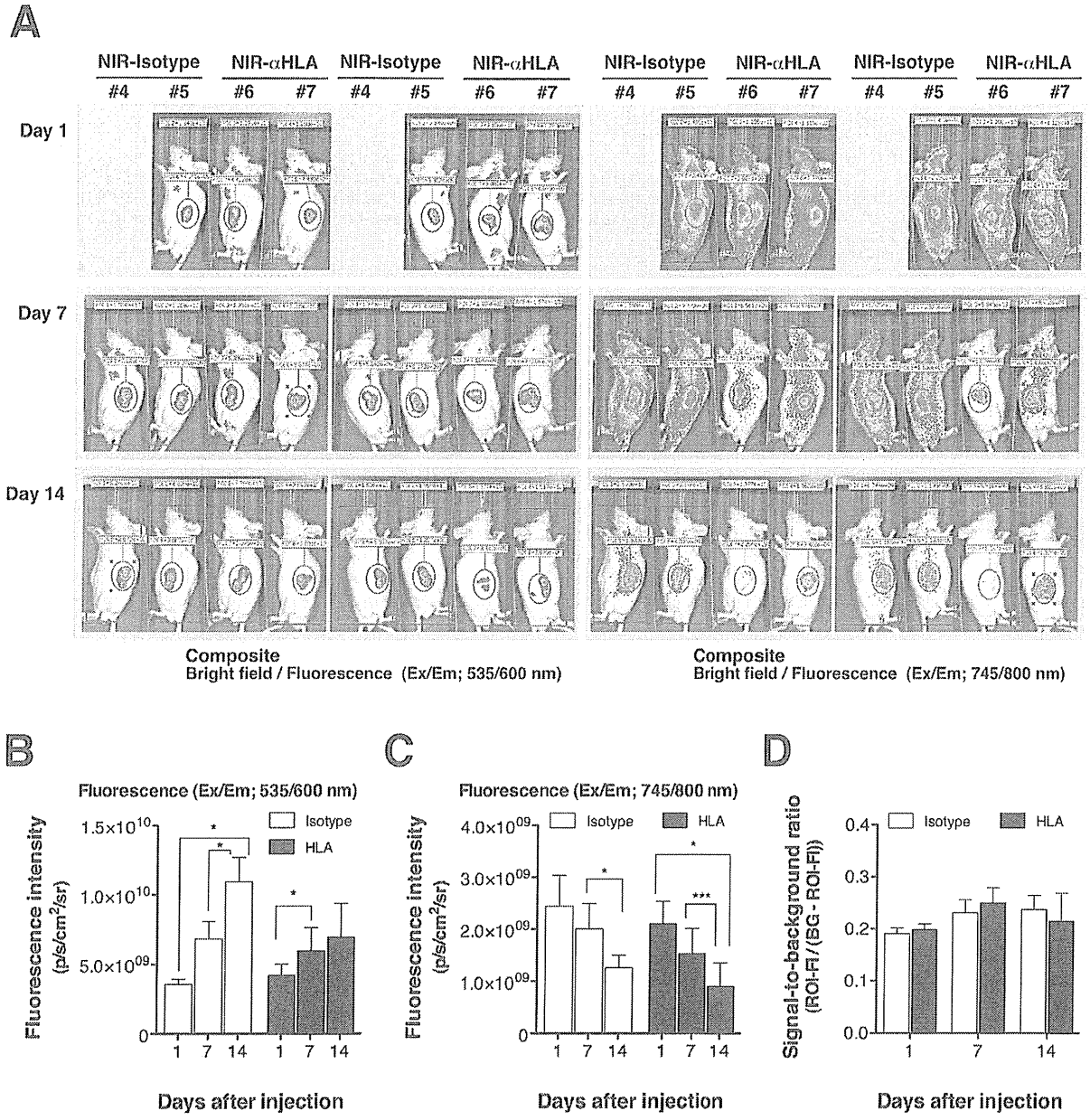

Figure 4. Time course of fluorescence intensities in human tumor xenografts after *iv* injection of NIR-conjugated macromolecule probes. (A) The fluorescent signal from the tdTomato (left panels) and NIR-probes (right panels) in subcutaneous T-HCT 116 tumor-bearing BRG nude mice (left and right flank, respectively) were detected at 1, 7, and 14 days after *iv* injection with NIR-probes, at wavelengths of 535/600 nm and 745/800 nm, respectively, using an IVIS SpectrumCT. (B) Fluorescence intensities of the tdTomato signal were quantified using ROIs of equivalent-sized areas from the tumor regions at the indicated time points (Student's *t* test, NIR-Isotype probe injected: $^{*}p$ value for 1 day and 14 days = 0.0216 and for 7 days and 14 days = 0.0126; NIR-αHLA probe injected: $^{*}p$ value for 1 day and 7 days = 0.0299). (C) Fluorescence intensities of the NIR-probe signal were quantified using ROIs of equivalent-sized areas from the tumor regions at the indicated time points (Student's *t* test, NIR-Isotype probe injected: $^{*}p$ value for 7 days and 14 days = 0.0176; NIR-αHLA probe injected: $^{*}p$ value for 1 day and 14 days = 0.0172, and $^{***}p$ value for 7 days and 14 days<0.0001). Data were presented as the mean ± SD of four individual tumors (two individual tumors in case of day1-#4 mouse. (D) The signal-to-background ratio (S/B) at 1, 7, and 14 days post-administration of the NIR-probes was calculated using the following formula: S/B = (fluorescence intensity of ROI)/((background intensity) – (fluorescence intensity of ROI)). In each case, the background was derived from equivalently sized areas containing the same number of pixels.
doi:10.1371/journal.pone.0082708.g004

that this optical imaging system could detect both fluoroprobes simultaneously with no cross-interference. Figure 3C shows a series of whole-body (left panels), dermabrasion (center panels), and *ex vivo* (right panels) fluorescence images that were obtained 24 hr after the administration of the NIR-Isotype or NIR-αHLA probes (90 μg/mouse). The specificity of the NIR-conjugated

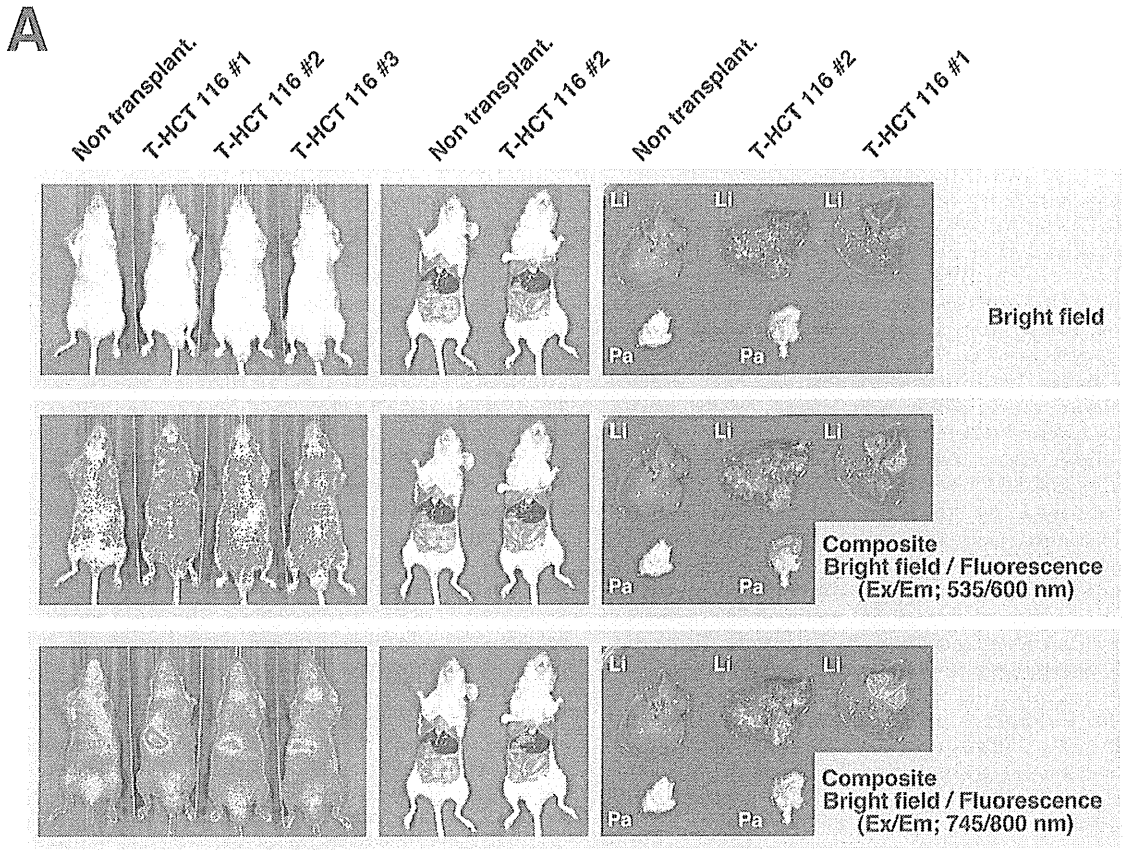
A
Non transplant.
T-HCT 116 #1
T-HCT 116 #2
T-HCT 116 #3
Non transplant.
T-HCT 116 #2
Non transplant.
T-HCT 116 #2
T-HCT 116 #1
Li
Pa
Bright field
Composite
Bright field / Fluorescence
(Ex/Em; 535/600 nm)
Composite
Bright field / Fluorescence
(Ex/Em; 745/800 nm)
B
RFP
MIgG2a
Non transplant.
T-HCT 116 #2
T-HCT 116 #1
2 mm
RFP
MIgG2a

Figure 5. *In vivo* imaging of the liver metastasis model with the NIR-αHLA probe. (A) *In vivo* fluorescence images of T-HCT 116 tumor-bearing BRG nude mice. The NIR fluorescence intensity 24 hr after *iv* injection of the NIR-αHLA probe can be observed using an IVIS SpectrumCT. The fluorescent signal from tdTomato and the NIR-αHLA probe were specifically detected at wavelengths of 535/600 nm and 745/800 nm, respectively. Nontransplant indicates that the BRG mouse had not received the T-HCT 116 cell transplant. Li; liver, Pa; pancreas. (B) Immunohistochemical staining of dissected livers; anti-RFP (RFP; left), and anti-mouse IgG_{2a} ($MIgG_{2a}$; right); Enlarged view of boxed area shown below. Scale bar, 200 μm.
doi:10.1371/journal.pone.0082708.g005

macromolecule probe for human tumors was demonstrated by the co-localization of the NIR and orange-red fluorescence signals within engrafted T-HCT 116 cells *in vivo* and *ex vivo*. The specific accumulation of the NIR-conjugated macromolecule probes within the T-HCT 116 xenograft was confirmed by immunohistochemical staining with anti-RFP antibody and anti-mouse immunoglobulin antibody. The injected NIR-conjugated macromolecule probes (mouse immunoglobulin G_{2a}) were localized around blood vessels, which were stained by the specific endothelial marker CD31 (Figure 3D).

The human tumors engrafted in BRG nude mice were successfully visualized by the NIR-Isotype probe and NIR-αHLA probes. To compare the NIR-Isotype and NIR-αHLA probes in terms of their ability to detect human tumor cells *in vivo*, the ROIs of that the fluorescence intensities of T-HCT 116 tumor and of background signal were quantified at different time points after probe administration (Figure 4). In contrast to the increasing orange-red fluorescent signals in T-HCT 116 cells (Figure 4B), both NIR fluorescent signals decreased over time (Figure 4C). The fluorescence intensity ratio between the tumor and background for NIR-probes is defined as the signal-to-background (S/B) ratio. The S/B ratio of NIR-Isotype and NIR-αHLA did not show significant differences between time points (Figure 4D). This result indicates that fluorescence imaging with the NIR-conjugated αHLA antibody was mainly based on the EPR effect.

NIR-conjugated macromolecule probes facilitate visualization of human tumors in various transplantation models

Following these initial proof of principle experiments, the NIR-conjugated macromolecule probes were used as imaging probes in subsequent experiments using various types of xenotransplantation models in BRG nude mice. We first attempted to detect the liver metastasis of colorectal cancer generated by the *isp* injection of T-HCT 116 cells. Three weeks after transplantation, the mice were treated with the NIR-αHLA probe (90 μg/mouse). Figure 5A shows a series of whole-body (left panels) and laparotomized body (center panels) fluorescence images from mice inoculated with T-HCT 116 cells, as well as *ex vivo* (right panels) fluorescence images. These pre- and post-mortem images were obtained 24 hr after administration of the NIR-αHLA probe. The fluorescence intensities observed in the mouse livers were higher than those in the rest of the body using fluorescence imaging with the 745/800 nm filter set in all T-HCT 116 cell–transplanted mice (3 out of 3). By contrast, we did not visualize the orange-red fluorescent signal of the liver-metastasized T-HCT 116 cells with the 535/600 nm filter set. *Ex vivo* imaging with the NIR-αHLA probe also demonstrated a clear demarcation of the tumor from the surrounding healthy liver tissue (Figure 5A, bottom panels). Furthermore, the NIR fluorescent signals were coincident with the orange-red fluorescent signal of the T-HCT 116 cells in *ex vivo* imaging. This specific accumulation of the NIR-αHLA probe in the liver-metastasized T-HCT 116 xenografts was confirmed by immunohistochemical staining with anti-RFP antibody and anti-mouse IgG_{2a} antibody (Figure 5B). The NIR-αHLA probes, which were detected by anti-mouse IgG_{2a} antibody, were localized within T-HCT 116 xenograft tumors, which were stained with anti-RFP antibody.

In subsequent experiments, we attempted to detect LC11-JCK xenograft tumors, which were established from human surgical specimens by serial passage in the subcutaneous spaces of immunodeficient BALB/cA nude mice. Recently, this type of tumor resource has been called a "Patient-Derived tumor Xenograft (PDX) model" [19]. To apply our versatile technique for *in vivo* imaging to the PDX model, 9 pieces of a 1-mm cubically dissected LC11-JCK xenograft were implanted into the subcutaneous spaces of BRG nude mice. After 4 weeks, the mice were treated with the NIR-αHLA probe or NIR-Isotype probes. Figure 6A shows a series of whole-body images that were obtained 2 days after administration of the NIR-probes. A bright-field image is shown in the top panel. When the fluorescent signals are overlaid onto the bright-field image, *in vivo* maintenance of the xenograft tumors can be visualized using both the NIR-αHLA and the NIR-Isotype probes. Dermabrasion and *ex vivo* fluorescence imaging with the NIR-conjugated macromolecule probes confirmed specific detection of the LC11-JCK tumors in whole-body imaging of the PDX model.

In the same manner as in the PDX model, we attempted to detect non-genetically modified HCT 116 cells by using NIR-conjugated macromolecule probes in various types of xenotransplantation models. We attempted to detect the unpredictable metastases of HCT 116 cells following *iv* injection of the cells. Four weeks after inoculation, the mice were treated with the NIR-αHLA probe (90 μg/mouse). Figure 6B shows a series of whole-body (left panels) and *ex vivo* laparotomized body (right panels) fluorescence images of mice inoculated with HCT 116 cells. These pre- and post-mortem images were obtained 2 days after administration of the NIR-αHLA probe. In the hematogenous metastasis model, following *iv* inoculation with HCT 116 cells, the development of renal metastases was detected noninvasively using this method. An orthotopic model of pancreatic cancer was prepared through a modified intrasplenic transplantation of BxPC-3 cells. Four weeks after transplantation, the mice were treated with the NIR-αHLA probe. Figure 6C shows a series of whole-body (left panels) and *ex vivo* laparotomized body (right panels) fluorescence images from mice inoculated with 1×10^6 BxPC-3 cells. Pre- and post-mortem images were obtained 2 days after the administration of NIR-αHLA probe (90 μg/mouse). In the whole-body imaging experiments, fluorescent signals were observed in areas similar to those observed in the renal metastasis model. However, the *ex vivo* laparotomized body fluorescence imaging revealed that the NIR fluorescent signals were located in the pancreas.

Discussion

This study demonstrates that whole-body optical imaging using NIR-conjugated macromolecule probes can detect human tumors in immunodeficient mice.

In vivo analyses of the growth and metastases of xenografts are crucial to the evaluation of new anti-cancer drugs and to the identification of molecules that play key roles in tumor malignancy. In experiments using subcutaneous xenograft models, measur-

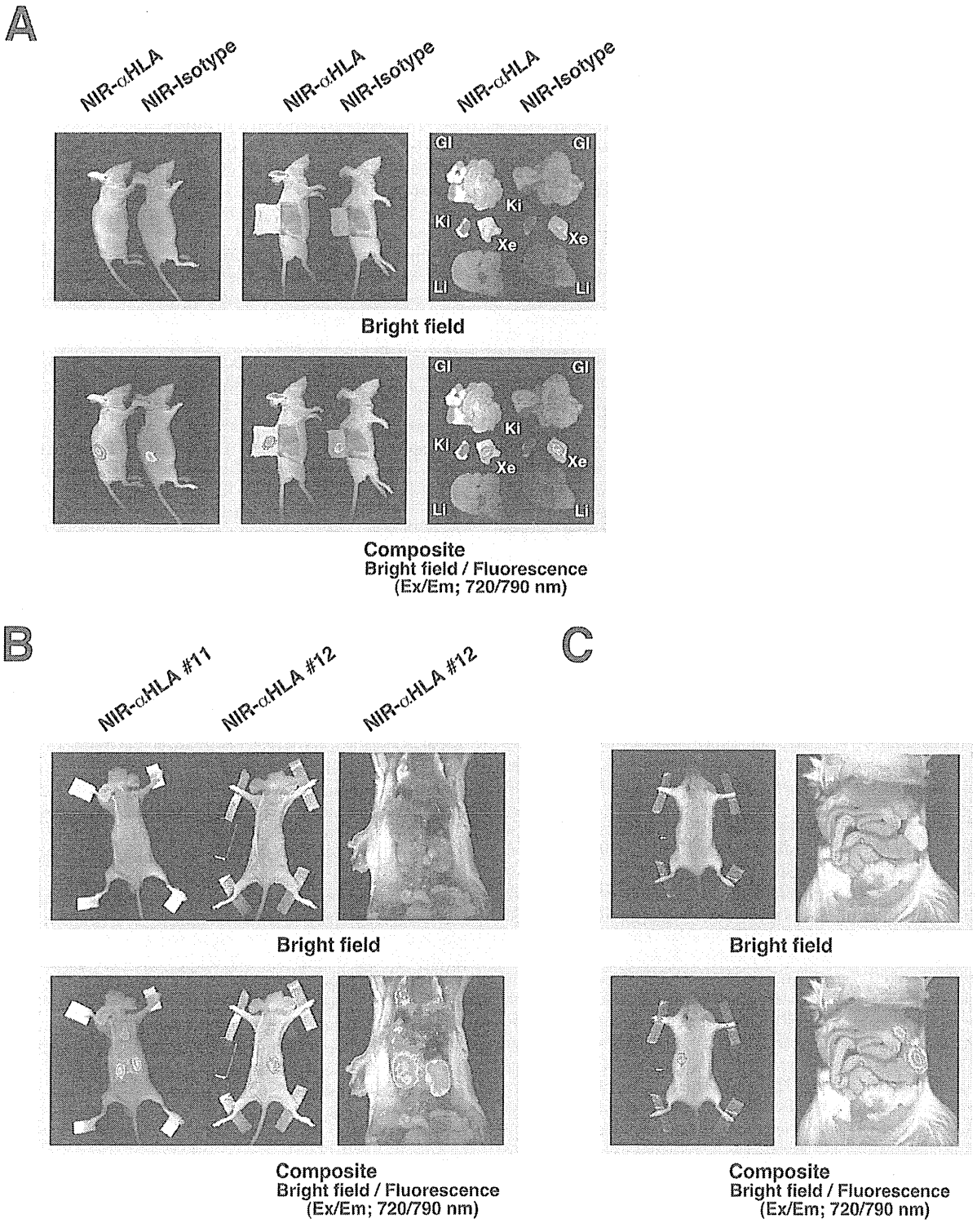

Figure 6. *In vivo* imaging with the NIR-αHLA probe detected human tumors in various transplantation models. (A) *In vivo* fluorescence images of BRG nude mice that had been implanted with small pieces of LC11-JCK xenograft tumors were taken 48 hr after *iv* injection with the NIR-αHLA probe or the NIR-Isotype probe (left panels). In laparotomized body *ex vivo* fluorescence images (center panels) and *ex vivo* fluorescence images (right panels), the fluorescent signal was specifically detected at wavelengths of 720/790 nm using the Kodak *In-Vivo* Imaging System FX. GI; gastrointestinal tract, Ki; kidney, Xe; LC11-JCK tumor xenograft, Li; liver. (B) *In vivo* fluorescence images of BRG nude mice that had received an intravenous (via tail-vein) injection of 1×10^5 HCT 116 cells were taken 48 hr after *iv* injection with the NIR-αHLA probe (left panels). Laparotomized

body *ex vivo* fluorescence images (right panels) are also shown. A bright-field image is shown in the top panel, a fluorescence image is shown in the center panel, and the composite image is shown in the right panel. (C) An *in vivo* fluorescence image of a NOG mouse that had received an intrasplenic injection of 1×10^6 BxPC-3 cells was taken 48 hr after *iv* injection with the NIR-αHLA probe (left panels). Laparotomized body *ex vivo* fluorescence images (right panels) are also shown. The fluorescent signal from the NIR-probes was acquired using the Kodak *In-Vivo* Imaging System FX.

doi:10.1371/journal.pone.0082708.g006

ing tumor volume can offer a clear evaluation of drug efficacy. In contrast, although orthotopic implantations and hematogenous metastasis models are more accurate [20], drug efficacy, particularly the tumor-suppressing effect of the drug, is evaluated only by autopsy or overall survival. These methods are invasive and time-consuming. In 2000, Yang et al. published a groundbreaking report on whole-body optical imaging using green fluorescent protein (GFP)-expressing cancer cells [21]. This work allowed unprecedented continuous, noninvasive visual assessments of malignant growth and spread in live animals. Tracking the GFP-expressing cancer cells *in vivo* is far more sensitive and rapid than cumbersome histological or immunohistochemical procedures [22]. Recently, the use of near-infrared (NIR) wavelengths (700–900 nm) instead of visible wavelengths (400–700 nm) was found to be advantageous for *in vivo* imaging, owing to the very low autofluorescence of tissue and the high level of tissue penetration of these wavelengths [23,24]. Although, we failed to visualize liver metastasis of tdTomato-expressing HCT 116 human colorectal cancer (T-HCT-116) cells by orange-red fluorescent protein tdTomato with the 535/600 nm filter set, the fluorescent signal from liver-metastasized T-HCT 116 cells was clearly detected by both NIR-αHLA (Figure 5A) and NIR-Isotype (data not shown) probes with the 745/800 nm filter set. This result confirmed that the NIR wavelength is superior to the orange-red fluorescence wavelength in terms of tissue penetration. To overcome the disadvantage of using tdTomato fluoroprotein, the spectra of the fluorescent proteins should be shifted to longer wavelengths. The infrared fluorescent protein alternative to GFP was originally isolated from *D. radiodurans* and showed superior utility in whole-body imaging of internal mammalian tissues [25,26]. However, the issue of which fluorescent protein expressing cell lines need to be established remains.

Solid tumors characteristically exhibit an accumulation of macromolecules, as a result of the EPR effect, which arises from the leaky vasculature within the tumors [9,10]. In this study, we examined the uptake of NIR-probes of different molecular sizes by conjugating the NIR fluorochrome to glycine (75 Da), BSA (67 kDa), and immunoglobulins (150 kDa). The NIR-conjugated macromolecules, including NIR-BSA, NIR-Isotype, and NIR-αHLA probe, accumulated in both BxPC-3 and HCT 116 xenograft tumors; in contrast, small molecular NIR-probes, such as NIR-glycine and free NIR fluorochrome, could not be retained in either the BxPC-3 or HCT 116 xenograft tumors (Figure 2). These results indicate that the principal mechanism underlying optical imaging with the NIR-conjugated macromolecule probes may be due to the EPR effect. Immunohistochemical staining with anti-mouse immunoglobulin G_{2a} revealed the localization of NIR-αHLA probes that had leaked from blood vessels. This localization supports the idea that the EPR effect, caused by leaky vasculature within the tumor, is the underlying mechanism [9,10].

In the subcutaneous transplantation model, all T-HCT 116 xenografts expressing orange-red fluorescence protein were successfully detected at both the Ex/Em 535/600 nm (tdTomato fluorescence reporter) and Ex/Em 745/800 nm (NIR-probe fluorescence) wavelengths (6 out of 6). In addition, all visible and palpable BxPC-3 and HCT 116 xenografts were also detected by NIR-probes (3/3 and 5/5, respectively). In a liver metastasis model with T-HCT 116 reporter cells, whole-body imaging with the 535/600 nm wavelength filter set failed to visualize liver-metastasized T-HCT 116 cells (0 out of 3). In contrast, the BRG nude mice that received *isp* transplantation with T-HCT 116 reporter cells emitted sufficient NIR fluorescent signal from the abdomen in whole-body imaging (3 out of 3). *Ex vivo* imaging of the liver metastasis model clearly demarcated tumors from the surrounding liver cells during detection of the fluorescent signal with both Ex/Em 535/600 nm and 745/800 nm wavelengths.

Using *ex vivo* imaging, but not whole-body imaging, we identified a mouse in which the intrasplenically transplanted T-HCT 116 cells had metastasized to the pancreas. Generally, it is known that the EPR-effect can be observed in almost all human cancers with the exception of hypovascular tumors such as prostate cancer or pancreatic cancer [27]. This characteristic might explain the unsuccessful detection of an NIR fluorescent signal in the tumor xenografts formed in the pancreas. Alternatively, the NIR fluorescent signal in xenograft tumors formed in the pancreas might be masked by the strong NIR fluorescent signal of liver-metastasized tumors. This hypothesis is supported by the successful whole-body imaging, using the NIR-αHLA probe, of the human pancreatic cancer (BxPC-3) xenograft formed in the pancreas(Figure 6C).

In human tumor xenografts and human tissue or cell transplantation models, anti-human HLA antibodies are powerful tools for detecting and distinguishing human cells from recipient mouse cells using immunohistochemical staining of tissue sections [13,14]. In this study, we confirmed that *in vitro*, the human cancer cell lines HCT 116 and BxPC-3 were specifically detected by NIR-conjugated anti-HLA antibody (NIR-αHLA probe) but not by NIR-conjugated isotype-matched immunoglobulin (NIR-Isotype probe). However, both NIR-probes had a similar capacity to detect the HCT 116 and BxPC-3 human cancer cells *in vivo*. This result indicates that fluorescence imaging with NIR-conjugated anti-HLA antibody *in vivo* is mainly based on the EPR effect rather than antigen–antibody binding. The BRG nude strain, which lacks immunoglobulin [28], might have an EPR effect-prone internal environment. It is known that some cancer cells have lost the surface expression of HLA molecules. However, the complete loss of HLA class I molecules was found to occur in only 9% (6 of 70) of a group of esophageal squamous cell carcinoma (ESCC) patients and was not observed (0 of 34) in a group of head and neck squamous cell carcinoma (HNSCC) patients [29,30]. Fortunately, our versatile method, which does not require any genetic modification of the target cancer cells, allows us to detect tumor xenografts by using BRG nude mice as recipients, even for cancers that have lost the surface expression of HLA class I antigen.

In this report, we demonstrated a simple method for detecting human xenograft tumors in immunodeficient mice: using NIR-conjugated macromolecule (immunoglobulin) probes. This versatile method for the *in vivo* imaging of human tumor xenografts should facilitate studies of cancer growth and metastasis and accelerate the development of potential chemotherapeutic agents.

Acknowledgments

We thank M. Kuronuma, Y. Ando, S. Inoue, and K. Hioki for outstanding technical assistance with the animal experiments. We thank Drs. M. Ito and Y. Ohnishi for helpful discussions.

Author Contributions

Conceived and designed the experiments: HS. Performed the experiments: HS KK YH TI ES. Analyzed the data: HS MN. Contributed reagents/materials/analysis tools: TO HH. Wrote the paper: HS MN.

References

1. Chang CJ, Tai KF, Roffler S, Hwang LH (2004) The immunization site of cytokine-secreting tumor cell vaccines influences the trafficking of tumor-specific T lymphocytes and antitumor efficacy against regional tumors. J Immunol 173: 6025–6032.
2. Giavazzi R, Campbell DE, Jessup JM, Cleary K, Fidler IJ (1986) Metastatic behavior of tumor cells isolated from primary and metastatic human colorectal carcinomas implanted into different sites in nude mice. Cancer Res 46: 1928–1933.
3. Suemizu H, Monnai M, Ohnishi Y, Ito M, Tamaoki N, et al. (2007) Identification of a key molecular regulator of liver metastasis in human pancreatic carcinoma using a novel quantitative model of metastasis in NOD/SCID/gammacnull (NOG) mice. Int J Oncol 31: 741–751.
4. Hamada K, Monnai M, Kawai K, Nishime C, Kito C, et al. (2008) Liver metastasis models of colon cancer for evaluation of drug efficacy using NOD/Shi-scid IL2Rgammanull (NOG) mice. Int J Oncol 32: 153–159.
5. Bibby MC (2004) Orthotopic models of cancer for preclinical drug evaluation: advantages and disadvantages. Eur J Cancer 40: 852–857.
6. Troy T, Jekic-McMullen D, Sambucetti L, Rice B (2004) Quantitative comparison of the sensitivity of detection of fluorescent and bioluminescent reporters in animal models. Mol Imaging 3: 9–23.
7. Deliolanis NC, Kasmieh R, Wurdinger T, Tannous BA, Shah K, et al. (2008) Performance of the red-shifted fluorescent proteins in deep-tissue molecular imaging applications. J Biomed Opt 13: 044008.
8. Lin MZ, McKeown MR, Ng HL, Aguilera TA, Shaner NC, et al. (2009) Autofluorescent proteins with excitation in the optical window for intravital imaging in mammals. Chem Biol 16: 1169–1179.
9. Matsumura Y, Maeda H (1986) A new concept for macromolecular therapeutics in cancer chemotherapy: mechanism of tumoritropic accumulation of proteins and the antitumor agent smancs. Cancer Res 46: 6387–6392.
10. Greish K, Fang J, Inutsuka T, Nagamitsu A, Maeda H (2003) Macromolecular therapeutics: advantages and prospects with special emphasis on solid tumour targeting. Clin Pharmacokinet 42: 1089–1105.
11. Keereweer S, Mol IM, Kerrebijn JD, Van Driel PB, Xie B, et al. (2012) Targeting integrins and enhanced permeability and retention (EPR) effect for optical imaging of oral cancer. J Surg Oncol 105: 714–718.
12. Concha A, Esteban F, Cabrera T, Ruiz-Cabello F, Garrido F (1991) Tumor aggressiveness and MHC class I and II antigens in laryngeal and breast cancer. Semin Cancer Biol 2: 47–54.
13. Machida K, Suemizu H, Kawai K, Ishikawa T, Sawada R, et al. (2009) Higher susceptibility of NOG mice to xenotransplanted tumors. J Toxicol Sci 34: 123–127.
14. Hasegawa M, Kawai K, Mitsui T, Taniguchi K, Monnai M, et al. (2011) The reconstituted 'humanized liver' in TK-NOG mice is mature and functional. Biochem Biophys Res Commun 405: 405–410.
15. Traggiai E, Chicha L, Mazzucchelli L, Bronz L, Piffaretti JC, et al. (2004) Development of a human adaptive immune system in cord blood cell-transplanted mice. Science 304: 104–107.
16. Isaacson JH, Cattanach BM (1962) Mouse News Letter 27: 31.
17. Ito M, Hiramatsu H, Kobayashi K, Suzue K, Kawahata M, et al. (2002) NOD/SCID/gamma(c)(null) mouse: an excellent recipient mouse model for engraftment of human cells. Blood 100: 3175–3182.
18. Oshika Y, Nakamura M, Abe Y, Fukuchi Y, Yoshimura M, et al. (1998) Growth stimulation of non-small cell lung cancer xenografts by granulocyte-macrophage colony-stimulating factor (GM-CSF). Eur J Cancer 34: 1958–1961.
19. Moro M, Bertolini G, Tortoreto M, Pastorino U, Sozzi G, et al. (2012) Patient-derived xenografts of non small cell lung cancer: resurgence of an old model for investigation of modern concepts of tailored therapy and cancer stem cells. J Biomed Biotechnol 2012: 568567.
20. Hoffman R (1999) Orthotopic metastatic mouse models for anticancer drug discovery and evaluation: a bridge to the clinic. Invest New Drugs 17: 343–359.
21. Yang M, Baranov E, Jiang P, Sun FX, Li XM, et al. (2000) Whole-body optical imaging of green fluorescent protein-expressing tumors and metastases. Proc Natl Acad Sci U S A 97: 1206–1211.
22. Bouvet M, Yang M, Nardin S, Wang X, Jiang P, et al. (2000) Chronologically-specific metastatic targeting of human pancreatic tumors in orthotopic models. Clin Exp Metastasis 18: 213–218.
23. Luo S, Zhang E, Su Y, Cheng T, Shi C (2011) A review of NIR dyes in cancer targeting and imaging. Biomaterials 32: 7127–7138.
24. Zhang X, Bloch S, Akers W, Achilefu S (2012) Near-infrared molecular probes for in vivo imaging. Curr Protoc Cytom Chapter 12: Unit12 27.
25. Shu X, Royant A, Lin MZ, Aguilera TA, Lev-Ram V, et al. (2009) Mammalian expression of infrared fluorescent proteins engineered from a bacterial phytochrome. Science 324: 804–807.
26. Filonov GS, Piatkevich KD, Ting LM, Zhang J, Kim K, et al. (2011) Bright and stable near-infrared fluorescent protein for in vivo imaging. Nat Biotechnol 29: 757–761.
27. Maeda H, Bharate GY, Daruwalla J (2009) Polymeric drugs for efficient tumor-targeted drug delivery based on EPR-effect. Eur J Pharm Biopharm 71: 409–419.
28. Goldman JP, Blundell MP, Lopes L, Kinnon C, Di Santo JP, et al. (1998) Enhanced human cell engraftment in mice deficient in RAG2 and the common cytokine receptor gamma chain. Br J Haematol 103: 335–342.
29. Mizukami Y, Kono K, Maruyama T, Watanabe M, Kawaguchi Y, et al. (2008) Downregulation of HLA Class I molecules in the tumour is associated with a poor prognosis in patients with oesophageal squamous cell carcinoma. Br J Cancer 99: 1462–1467.
30. Vora AR, Rodgers S, Parker AJ, Start R, Rees RC, et al. (1997) An immunohistochemical study of altered immunomodulatory molecule expression in head and neck squamous cell carcinoma. Br J Cancer 76: 836–844.

A new *in vivo* model to analyze hepatic metastasis of the human colon cancer cell line HCT116 in NOD/Shi-*scid*/IL-2Rγ^{null} (NOG) mice by ^{18}F-FDG PET/CT

KENJI KAWAI[1], KATSUMI TAMURA[3], IKUKO SAKATA[3], JIRO ISHIDA[3], MASAYOSHI NAGATA[4], HIDEO TSUKADA[5], HIROSHI SUEMIZU[2], MASATO NAKAMURA[1,6], YOSHIYUKI ABE[3] and TSUYOSHI CHIJIWA[1]

[1]Pathology Research Department, [2]Biomedical Research Department, Central Institute for Experimental Animals, Kawasaki, Kanagawa 210-0821; [3]Tokorozawa PET Diagnostic Imaging Clinic, Tokorozawa, Saitama 359-1124; [4]Iruma Heart Hospital, Iruma, Saitama 358-0026; [5]Central Research Laboratory, Hamamatsu Photonics K.K., Hamamatsu, Shizuoka 434-8601; [6]Department of Regenerative Medicine and Pathology, Tokai University School of Medicine, Isehara, Kanagawa 259-1193, Japan

Received September 10, 2012; Accepted October 23, 2012

DOI: 10.3892/or.2012.2141

Abstract. Clinically, ^{18}F-fluorodeoxyglucose positron emission tomography/computed tomography (^{18}F-FDG-PET/CT) is useful in the evaluation of various types of human cancers. While PET analysis has been established to evaluate subcutaneous lesions of human cancers in mice, its applications for internal lesions are still being developed. We are currently evaluating new PET approaches for the effective evaluation of *in vivo* metastatic lesions in the internal organs of small experimental animals. In this study, we analyzed *in vivo* hepatic metastases of human colonic cancer in immunodeficient mice (NOD/Shi-*scid*/IL-2Rγ^{null}, NOG) using PET imaging. This new PET approach has been proposed for the evaluation of *in vivo* metastatic lesions in internal organs. The human colon cancer line HCT116 ($1.0x10^5$ and $1.0x10^6$ cells/mouse) was transplanted by intrasplenic injection. ^{18}F-FDG-PET/CT scans were performed 2 weeks after transplantation. After PET/CT scans, histopathological examinations were performed. PET/CT analysis disclosed multiple metastatic foci and increased standardized uptake values (SUV) of FDG in the livers of NOG mice (control, SUVmean 0.450±0.033, SUVmax 0.635±0.017; $1.0x10^5$ cells, 0.853±0.087, 1.254±0.237; $1.0x10^6$ cells, 1.211±0.108, 1.701±0.158). There were significant differences in FDG uptakes between the three groups (ANOVA, P=0.017 in SUVmean; P=0.044 in SUVmax, n=2). We clearly and quantitatively detected images of hepatic metastasis in the livers of NOG mice by ^{18}F-FDG-PET/CT *in vivo*. PET/CT analysis of internal organ lesions of human cancerous xenografts is a new reliable experimental system to simulate metastases. This model system is useful for analyzing metastatic mechanisms and for developing new novel drugs targeting hepatic metastases of cancer.

Correspondence to: Dr Tsuyoshi Chijiwa, Pathology Research Department, Central Institute for Experimental Animals, 3-25-12 Tonomachi, Kawasaki-ku, Kawasaki, Kanagawa 210-0821, Japan
E-mail: chijiwa@ciea.or.jp

Key words: ^{18}F-FDG, PET, NOG mouse, colon cancer, tumor xenograft

Introduction

Chemotherapy has contributed to improvements in the outcome of colorectal cancer (1,2), yet the control of metastatic lesions is crucial for improving outcomes. The metastatic mechanisms of colon cancer are still not known in detail; however, previous studies by us and others have identified the key molecules related to liver metastasis in colon cancer (3-5), and pathological findings of budding and venous invasion of tumors are known to be important in predicting the outcome of colorectal cancer (6,7). Clinically, ^{18}F-fluorodeoxyglucose positron emission tomography/computed tomography (^{18}F-FDG-PET/CT) fusion imaging is a useful tool for evaluating the stage, recurrence, outcome, and effectiveness of treatment in human cancers (8-11). Some studies have reported that PET/CT is useful in colon cancer (12-14). However, PET/CT imaging has a limitation in revealing hepatic metastasis due to normal uptake in the liver (15).

Many studies have shown that *in vivo* studies with subcutaneous xenografts in nude mice and severe combined immunodeficient (SCID) mice are useful for analyzing human cancers (16-19), whereas they are limited in evaluating internal organ metastases associated with human cancers. Immunodeficient mice commonly show poor metastatic lesions *in vivo*. We reported that distant metastatic lesions were easily reproduced by human cancer cell lines in newly developed NOD/Shi-*scid*/IL-2Rγ^{null} (NOG) mouse models employing systemic injections (20-23). It was confirmed that

the experimental metastasis model of human cancer using NOG mice was more sensitive and easier to achieve than that using SCID mice due to their multiple immunological dysfunctions not only in cytokine production capability, but also in the functional competence of T, B and NK cells (24,25). We previously developed a reliable new model for assaying hepatic metastasis with superimmunodeficient NOG mice (26,27).

Some *in vivo* studies have evaluated metastatic lesions of internal organs in mice with conventional modalities such as bio-luminescence imaging (BLI), but difficulties were found in revealing the mechanisms of metastasis (28). Therefore, a new *in vivo* system to detect internal organ metastatic lesions is required to simulate the clinical situation of metastatic lesions using reliable and quantitative approaches.

In this study, we examined whether ^{18}F-FDG-PET/CT scans could semi-quantitatively reveal abnormal FDG uptakes in hepatic metastasis of human colon cancer cell line HCT116 in NOG mice, thereby overcoming the above described limitations encountered when evaluating metastatic lesions in the liver. Moreover, liver metastasis in NOG mice was studied by histopathological analysis. We showed here that the evaluation of metastatic lesions in NOG mice by PET/CT may be an extremely useful *in vivo* metastatic model.

Materials and methods

Cell culture. The HCT116 cell line was obtained from the American Type Culture Collection (Manassas, VA, USA) and maintained in McCoy's 5A medium (Sigma-Aldrich, St. Louis, MO, USA) supplemented with 10% heat-inactivated fetal bovine serum, 100 U/ml penicillin and 100 μg/ml streptomycin. Cells were incubated in a humidified (37°C, 5% CO_2) incubator and passaged on reaching 80% confluence.

In vivo transplantation of human colon cancer cell line, HCT116. NOG mice (9-12 weeks of age, male) were maintained at the specific pathogen-free facilities of the Central Institute for Experimental Animals (CIEA, Kawasaki, Japan). Experimental liver metastases using NOG mice were generated by intrasplenic injection of HCT116 cells ($1.0x10^5$ and $1.0x10^6$/mouse, n=2) and splenectomy. All experiments involving laboratory animals were performed in accordance with the care and use guidelines of the CIEA, according to our previous reports (26,27).

Whole-body imaging of NOG mice with ^{18}F-FDG-PET and CT scans. Positron-emitting fluorine-18 (^{18}F) was produced by ^{18}O(p,n)^{18}F nuclear reaction using a cyclotron (HM-18; Sumitomo Heavy Industry, Osaka, Japan) at Hamamatsu Photonics PET Center. ^{18}F-FDG-PET and CT scans were performed in NOG mice 14 days after transplantation. The production of ^{18}F-FDG was carried out according to a method described elsewhere (29). The kinetics and distribution patterns of the radiolabeled compound were determined with a small animal PET scanner (ClairvivoPET; Shimadzu Corp., Kyoto, Japan). This scanner consists of depth of interaction (DOI) detector modules with an axial field of view (FOV) of 151 mm, a transaxial FOV of 102 mm, and a transaxial spatial resolution of 1.54 mm in the center (30). Anesthetized mice were placed in a prone position on a fixation plate and then placed in the gantry hole of the PET scanner. After transmission measurement with an external ^{137}Cs point source (22 MBq) for attenuation correction, ^{18}F-FDG at a dose of 6 MBq (0.2 ml) was injected intravenously into each mouse via the tail vein. Data were acquired in list-mode format for 60 min; full 3D sinograms with corrected efficiency, scattering, attenuation, count losses and decay were reconstructed using an iterative 3D dynamic raw-action maximum likelihood algorithm (Drama). Summation images from 40 to 60 min after ^{18}F-FDG injection were reconstructed, and average and maximum values of the standardized uptake (SUVmean, SUVmax) were semi-quantitatively calculated in various organs of NOG mice. After PET scanning, a CT scan was performed with ClairvivoCT (Shimadzu Corp.) in each NOG mouse.

Table I. SUV values in the various organs of control NOG mice by ^{18}F-FDG-PET/CT.

	SUVmean	SUVmax
Brain	1.519±0.083	2.140±0.127
Heart	1.343±0.035	1.868±0.016
Kidney	2.163±0.125	3.148±0.150
Bladder	32.986±3.590	49.692±8.152
Lung	0.577±0.064	1.384±0.104
Liver	0.450±0.033	0.635±0.017
Muscle	0.151±0.011	0.327±0.040
Bone	0.214±0.013	0.476±0.034
Intestine	0.824±0.033	2.061±0.111
Testis	0.510±0.022	1.212±0.335

Standardized uptake values (SUV) were examined by ^{18}F-FDG.

Macroscopic and microscopic examinations. Mice were autopsied after PET/CT scan examinations to evaluate liver metastases. These metastatic lesions were also histologically confirmed. Immunohistochemistry was carried out on 4 μm tissue sections using the Bond Polymer Refine Detection system (Leica Microsystems, Tokyo, Japan) according to the manufacturer's instructions with minor modifications. In brief, 4 μm sections of formalin-fixed, paraffin-embedded tissues were deparaffinized by Bond Dewax Solution (Leica Microsystems) and an antigen retrieval procedure was carried out using Bond ER solution (Leica Microsystems) for 30 min at 100°C. Endogenous peroxidases were quenched by incubation with hydrogen peroxide for 5 min. Sections were incubated for 30 min at ambient temperate with primary monoclonal antibodies for anti-HLA class 1-A, B, C (Hokudo, Sapporo, Japan) using the biotin-free polymeric horseradish peroxidase (HRP)-linker antibody conjugate system in a Bond-Max automatic slide stainer (Leica Microsystems). Nuclei were counterstained with hematoxylin.

Statistical analysis. Statistical comparisons of data sets were analyzed by a one-way factorial ANOVA. Data are shown as means ± standard error of mean (SEM). These analyses were performed using JMP version 8 software (SAS Institute, Inc., Cary, NC, USA). P-values <0.05 were considered to indicate statistically significant differences.

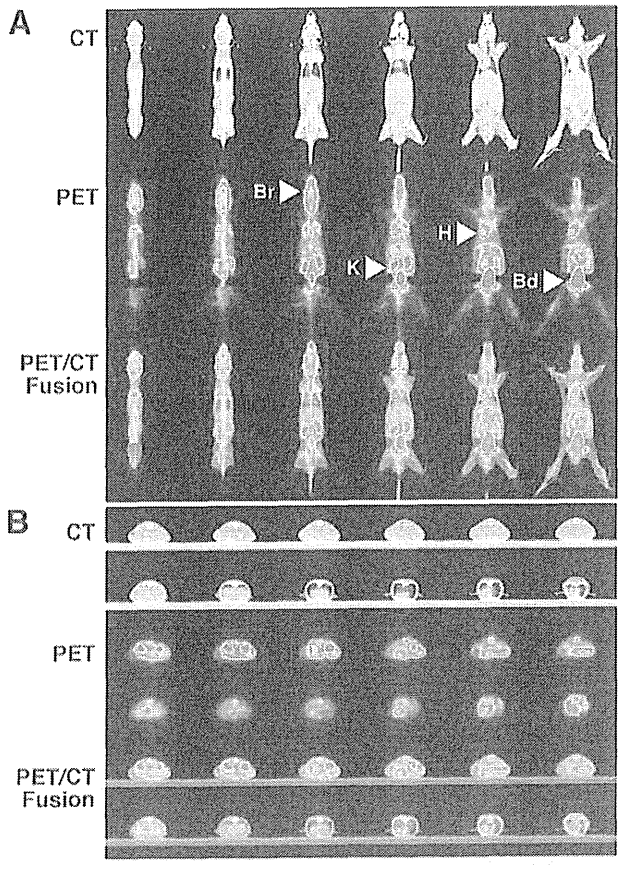

Figure 1. PET and CT findings in control NOG mice. FDG-PET/CT shows intense FDG uptakes in the brain (Br, SUVmax 2.140±0.127), heart (H, SUVmax 1.868±0.016), kidney (K, SUVmax 3.148±0.150) and bladder (Bd, SUVmax 49.692±8.152) of control NOG mice. (A) Coronal view, (B) axial view. Upper panels, CT; middle panels, PET; lower panels, PET/CT fusion.

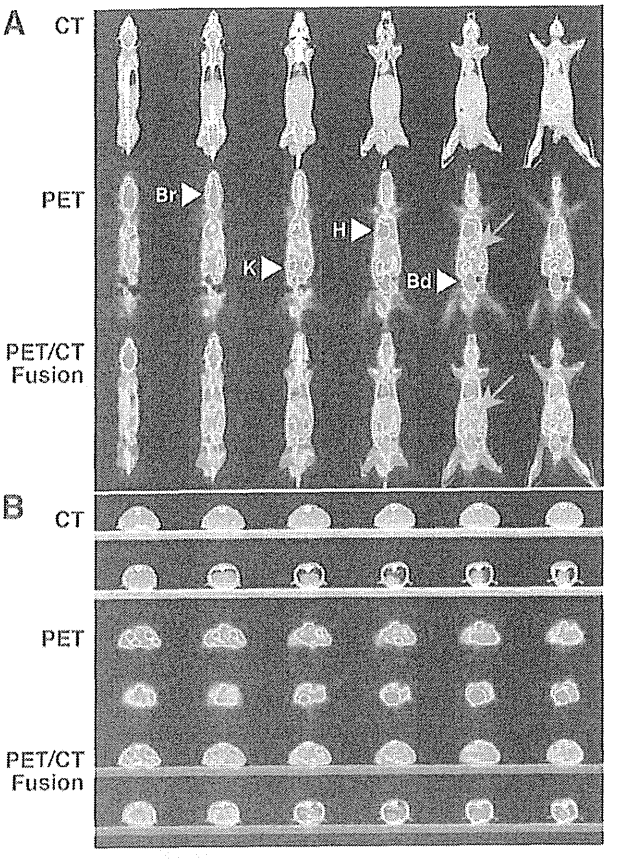

Figure 2. PET and CT findings in NOG mice transplanted with $1.0x10^5$ of HCT116 cells. FDG-PET/CT shows significantly increased multiple FDG uptakes (red arrow, SUVmax 1.017) in the livers of NOG mice transplanted with $1.0x10^5$ cells of the HCT116 cell line. (A) Coronal view, (B) axial view. Upper panels, CT; middle panels, PET; lower panels, PET/CT fusion. Br, brain; H, heart; K, kidney; Bd, bladder.

Results

^{18}F-FDG-PET findings in control NOG mice. ^{18}F-FDG-PET/CT showed intense FDG uptakes in the brain (SUVmean 1.519±0.083, SUVmax 2.140±0.127), heart (SUVmean 1.343±0.035, SUVmax 1.868±0.016), kidney (SUVmean 2.163±0.125, SUVmax 3.148±0.150) and bladder (SUVmean 32.986±3.590, SUVmax 49.692±8.152) of control NOG mice (Table I, Fig. 1).

^{18}F-FDG-PET and CT findings of tumor metastasis in NOG mice. ^{18}F-FDG-PET/CT showed higher multiple FDG uptakes (SUVmean 0.853±0.087, SUVmax 1.254±0.237) in the livers of NOG mice transplanted with $1.0x10^5$ cells of the HCT116 cell line (Table II, Fig. 2) than those of control NOG mice (SUVmean 0.450±0.033, SUVmax 0.635±0.017). CT scans also showed marked liver swelling in NOG mice transplanted with $1.0x10^6$ cells of HCT116 (Fig. 3). PET/CT showed diffuse higher FDG uptakes (SUVmean 1.211±0.108, SUVmax 1.701±0.158) in the livers of NOG mice with injection of $1.0x10^6$ HCT116 cells than FDG uptakes with $1.0x10^5$ cells. There were significant differences in FDG uptakes between the three groups (ANOVA, P=0.017 in SUVmean, P=0.044 in SUVmax). No other organs with abnormal FDG uptake were noted besides that of the livers of NOG mice transplanted with $1.0x10^5$ and $1.0x10^6$ cells of HCT116.

Table II. SUV values in the livers of NOG mice by ^{18}F-FDG-PET/CT.

	SUVmean	SUVmax
Control	0.450±0.033[a]	0.635±0.017[b]
$1.0x10^5$ cells of HCT116	0.853±0.087[a]	1.254±0.237[b]
$1.0x10^6$ cells of HCT116	1.211±0.108[a]	1.701±0.158[b]

Standardized uptake values (SUV) were examined by ^{18}F-FDG-PET/CT. ANOVA, [a]P=0.017, [b]P=0.044; n=2.

In vivo liver metastasis. Experimental liver metastases, which consisted of solid white masses, were detected in all livers of NOG mice transplanted with $1.0x10^5$ and $1.0x10^6$ cells of the HCT116 cell line. Metastatic hepatomegaly transplanted with $1.0x10^6$ cells was more severe than that with $1.0x10^5$ cells (Fig. 4, H&E). It was also immunohistochemically confirmed that there were obviously more metastatic foci in the livers of

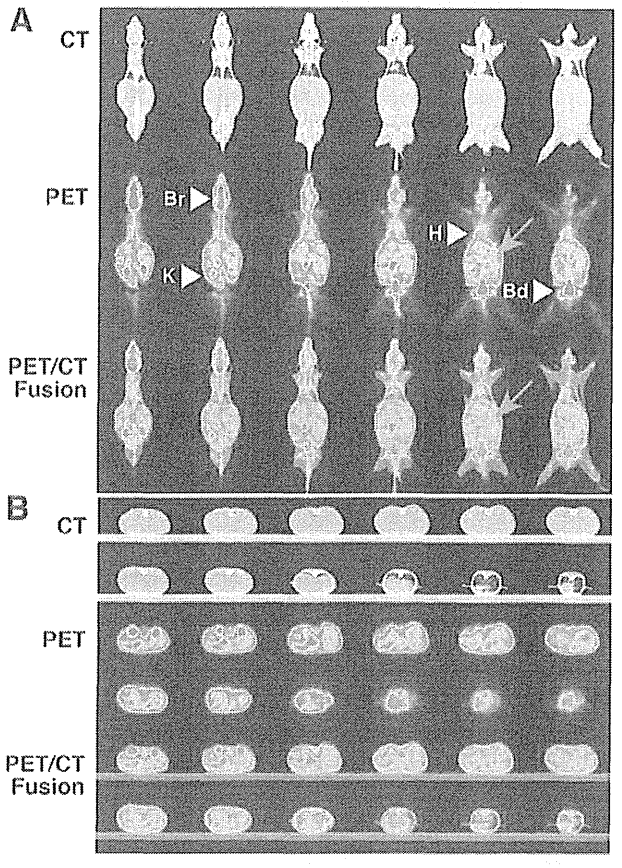

Figure 3. PET and CT findings in NOG mice transplanted with $1.0x10^6$ of HCT116 cells. CT scans show marked liver swelling in NOG mice transplanted with $1.0x10^6$ of HCT116 cells. PET/CT show diffuse higher FDG uptakes (red arrow, SUVmax 1.859) in livers. (A) Coronal view, (B) axial view. Upper panels, CT; middle panels, PET; lower panels, PET/CT fusion. Br, brain; H, heart; K, kidney; Bd, bladder.

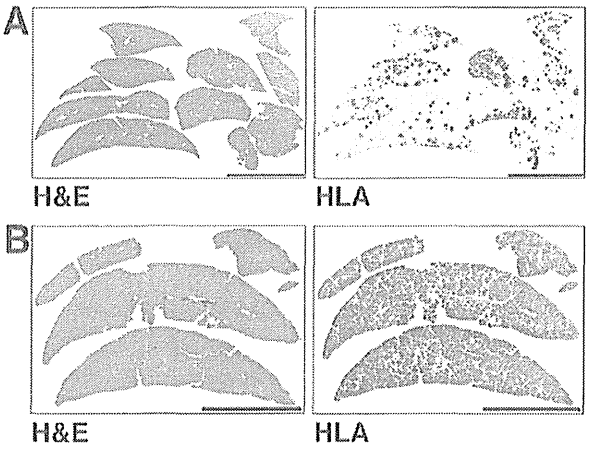

Figure 4. Histopathological findings of liver metastases. Experimental liver metastases in mice transplanted with both $1.0x10^5$ and $1.0x10^6$ of HCT116 cells showed metastatic hepatomegaly. Anti-HLA immunohistochemical examinations revealed that there were many more metastatic foci of human cancer in the livers of NOG mice transplanted with $1.0x10^6$ than foci in mice transplanted with $1.0x10^5$ of HCT116 cells. (A) $1.0x10^5$ HCT116 cells, (B) $1.0x10^6$ HCT116 cells; H&E, hematoxylin and eosin; HLA, anti-HLA immunohistochemistry; Scale bar, 5 mm.

NOG mice transplanted with $1.0x10^6$ than in mice transplanted with $1.0x10^5$ HTC116 cells (Fig. 4, HLA).

Discussion

In this study, we clearly and quantitatively demonstrated increased multiple ^{18}F-FDG uptakes in hepatic metastases of human colonic cancer cell line HCT116 in NOG mouse models using a small animal PET/CT system. We previously reported that ^{18}F-FDG-PET/CT clinically is a very useful imaging modality to evaluate human cancers, including rare carcinoma cases (31-34). Many reports have shown that animal PET imaging is useful for evaluating human cancer xenografts *in vivo*. It is usually difficult to reveal metastases as conventional *in vivo* models are limited in their evaluation of metastases associated with human cancers (28,35). It is easy to produce experimental liver metastases in immunocompromised NOG mice because of their multiple immunological dysfunctions in cytokine production capability as well as functional competence of T, B and NK cells (24-27). However, quantitative evaluation of experimental liver metastases is still being developed. We previously reported the use of liver weight as an index of metastatic hepatomegaly or microvessel counts to reflect tumor cell activity (23,36). We present herein that the model system with NOG mice and a small animal PET/CT system has the feasibility of a quantitative metastasis model to simulate clinical situations. Several studies have reported the development of new anticancer therapies and novel drugs for human cancers using animal PET (37,38). This model system presented here with NOG mice and a small animal PET/CT system may be useful for developing new anticancer therapies and novel drugs for hepatic metastases of human cancers.

Although PET imaging with ^{18}F-FDG is routinely used for tumor detection and therapy monitoring, several limitations have been reported with ^{18}F-FDG, such as high uptake in normal tissues of the brain and inflammatory tissues (15,39). In contrast, positron-labeled amino acids and their analogs are considered to be useful because of the low rate of amino acid use in normal control tissues. Natural and unnatural artificial labeled amino acids have been reported (40,41). This hepatic metastasis model, using intrasplenic injection of small numbers of cancer cells into NOG mice, is reliable and quantitative, and more closely mimics *in vivo* conditions (26). New compounds, which are more sensitive and specific for the detection of human cancers, are expected to replace ^{18}F-FDG (42,43). The hepatic metastasis model system in NOG mice combined with small animal PET/CT analysis will be useful in developing new labeling compounds for PET.

In conclusion, the hepatic metastasis model system in NOG mice combined with PET/CT has the feasibility to simulate clinical situations, and this model system is useful for analyzing mechanisms of metastasis and developing new therapeutic approaches for metastatic lesions of human cancers.

Acknowledgements

We are grateful to Hiroshi Iwata, Takeharu Kaiuchi, Norihiro Harada and Dai Fukumoto for their technical assistance and helpful discussions.

References

1. O'Connor ES, Greenblatt DY, LoConte NK, *et al*: Adjuvant chemotherapy for stage II colon cancer with poor prognostic features. J Clin Oncol 29: 3381-3388, 2011.
2. Karoui M, Roudot-Thoraval F, Mesli F, *et al*: Primary colectomy in patients with stage IV colon cancer and unresectable distant metastases improves overall survival: results of a multicentric study. Dis Colon Rectum 54: 930-938, 2011.
3. Tokunaga T, Oshika Y, Abe Y, *et al*: Vascular endothelial growth factor (VEGF) mRNA isoform expression pattern is correlated with liver metastasis and poor prognosis in colon cancer. Br J Cancer 77: 998-1002, 1998.
4. Tokunaga T, Nakamura M, Oshika Y, *et al*: Thrombospondin 2 expression is correlated with inhibition of angiogenesis and metastasis of colon cancer. Br J Cancer 79: 354-359, 1999.
5. Sun L, Hu H, Peng L, *et al*: P-cadherin promotes liver metastasis and is associated with poor prognosis in colon cancer. Am J Pathol 179: 380-390, 2011.
6. Tanaka M, Hashiguchi Y, Ueno H, Hase K and Mochizuki H: Tumor budding at the invasive margin can predict patients at high risk of recurrence after curative surgery for stage II, T3 colon cancer. Dis Colon Rectum 46: 1054-1059, 2003.
7. Sato T, Ueno H, Mochizuki H, *et al*: Objective criteria for the grading of venous invasion in colorectal cancer. Am J Surg Pathol 34: 454-462, 2010.
8. Cronin CG, Swords R, Truong MT, *et al*: Clinical utility of PET/CT in lymphoma. Am J Roentgenol 194: W91-W103, 2010.
9. Ueda S, Saeki T, Shigekawa T, *et al*: ^{18}F-fluorodeoxyglucose positron emission tomography optimizes neoadjuvant chemotherapy for primary breast cancer to achieve pathological complete response. Int J Clin Oncol 17: 276-282, 2012.
10. Xie L, Saynak M, Veeramachaneni NK, *et al*: Non-small cell lung cancer: prognostic importance of positive FDG PET findings in the mediastinum for patients with N0-N1 disease at pathologic analysis. Radiology 261: 226-234, 2011.
11. Abe Y, Tamura K, Sakata I, *et al*: Clinical implications of 18F-fluorodeoxyglucose positron emission tomography/computed tomography at delayed phase for diagnosis and prognosis of malignant pleural mesothelioma. Oncol Rep 27: 333-338, 2012.
12. Mori S and Oguchi K: Application of (18)F-fluorodeoxyglucose positron emission tomography to detection of proximal lesions of obstructive colorectal cancer. Jpn J Radiol 28: 584-590, 2010.
13. Ducreux M and Dromain C: Non-invasive imaging tools in colorectal cancer. Rev Prat 60: 1071-1073, 2010 (In French).
14. Treglia G, Calcagni ML, Rufini V, *et al*: Clinical significance of incidental focal colorectal (18)F-fluorodeoxyglucose uptake: our experience and a review of the literature. Colorectal Dis 14: 174-180, 2012.
15. Kubota R, Kubota K, Yamada S, Tada M, Ido T and Tamahashi N: Microautoradiographic study for the differentiation of intratumoral macrophages, granulation tissues and cancer cells by the dynamics of fluorine-18-fluorodeoxyglucose uptake. J Nucl Med 35: 104-112, 1994.
16. Abe Y, Nakamura M, Ohnishi Y, Inaba M, Ueyama Y and Tamaoki N: Multidrug resistance gene (MDR1) expression in human tumor xenografts. Int J Oncol 5: 1285-1292, 1994.
17. Abe Y, Ohnishi Y, Yoshimura M, *et al*: P-glycoprotein-mediated acquired multidrug resistance of human lung cancer cells in vivo. Br J Cancer 74: 1929-1934, 1996.
18. Suto R, Abe Y, Nakamura M, *et al*: P-glycoprotein-mediated acquired multidrug resistance of human osteosarcoma xenografts *in vivo*. Int J Oncol 12: 287-291, 1998.
19. Fujimori S, Abe Y, Nishi M, *et al*: The subunits of glutamate cysteine ligase enhance cisplatin resistance in human non-small cell lung cancer xenografts *in vivo*. Int J Oncol 25: 413-418, 2004.
20. Miyakawa Y, Ohnishi Y, Tomisawa M, *et al*: Establishment of a new model of human multiple myeloma using NOD/SCID/gamma(c)(null) (NOG) mice. Biochem Biophys Res Commun 313: 258-262, 2004.
21. Ikoma N, Yamazaki H, Abe Y, *et al*: S100A4 expression with reduced E-cadherin expression predicts distant metastasis of human malignant melanoma cell lines in the NOD/SCID/γ_c^{null} (NOG) mouse model. Oncol Rep 14: 633-637, 2005.
22. Hamada K, Monnai M, Kawai K, *et al*: Liver metastasis models of colon cancer for evaluation of drug efficacy using NOD/Shi-scid IL2Rγ^{null} (NOG) mice. Int J Oncol 32: 153-159, 2008.
23. Chijiwa T, Abe Y, Ikoma N, *et al*: Thrombospondin 2 inhibits metastasis of human malignant melanoma through microenvironment-modification in NOD/SCID/γ_c^{null} (NOG) mice. Int J Oncol 34: 5-13, 2009.
24. Ito M, Hiramatsu H, Kobayashi K, *et al*: NOD/SCID/gamma(c)(null) mouse: an excellent recipient mouse model for engraftment of human cells. Blood 100: 3175-3182, 2002.
25. Hiramatsu H, Nishikomori R, Heike T, *et al*: Complete reconstitution of human lymphocytes from cord blood CD34$^+$ cells using the NOD/SCID/gamma(c)(null) mice model. Blood 102: 873-880, 2003.
26. Suemizu H, Monnai M, Ohnishi Y, Ito M, Tamaoki N and Nakamura M: Identification of a key molecular regulator of liver metastasis in human pancreatic carcinoma using a novel quantitative model of metastasis in NOD/SCID/γ_c^{null} (NOG) mice. Int J Oncol 31: 741-751, 2007.
27. Kubo A, Ohmura M, Wakui M, *et al*: Semi-quantitative analyses of metabolic systems of human colon cancer metastatic xenografts in livers of superimmunodeficient NOG mice. Anal Bioanal Chem 400: 1895-1904, 2011.
28. Deroose CM, De A, Loening AM, *et al*: Multimodality imaging of tumor xenografts and metastases in mice with combined small-animal PET, small-animal CT, and bioluminescence imaging. J Nucl Med 48: 295-303, 2007.
29. Oberdorfer F, Hull WE, Traving BC and Maier-Borst W: Synthesis and purification of 2-deoxy-2-[18F]fluoro-D-glucose and 2-deoxy-2-[18F]fluoro-D-mannose: characterization of products by 1H- and 19F-NMR spectroscopy. Int J Rad Appl Instrum A 37: 695-701, 1986.
30. Mizuta T, Kitamura K, Iwata H, *et al*: Performance evaluation of a high-sensitivity large-aperture small-animal PET scanner: ClairvivoPET. Ann Nucl Med 22: 447-455, 2008.
31. Ueda S, Tsuda H, Asakawa H, *et al*: Clinicopathological and prognostic relevance of uptake level using 18F-fluorodeoxyglucose positron emission tomography/computed tomography fusion imaging (18F-FDG PET/CT) in primary breast cancer. Jpn J Clin Oncol 38: 250-258, 2008.
32. Abe Y, Tamura K, Sakata I, *et al*: Usefulness of ^{18}F-FDG positron emission tomography/computed tomography for the diagnosis of pyothorax-associated lymphoma: a report of three cases. Oncol Lett 1: 833-836, 2010.
33. Abe Y, Tamura K, Sakata I, *et al*: Unique intense uptake demonstrated by ^{18}F-FDG positron emission tomography/computed tomography in primary pancreatic lymphoma: a case report. Oncol Lett 1: 605-607, 2010.
34. Ozeki Y, Abe Y, Kita H, *et al*: A case of primary lung cancer lesion demonstrated by F-18 FDG positron emission tomography/computed tomography (PET/CT) one year after the detection of metastatic brain tumor. Oncol Lett 2: 621-623, 2011.
35. Takamiya Y, Abe Y, Tanaka Y, *et al*: Murine P-glycoprotein on stromal vessels mediates multidrug resistance in intracerebral human glioma xenografts. Br J Cancer 76: 445-450, 1997.
36. Hatanaka H, Oshika Y, Abe Y, *et al*: Vascularization is decreased in pulmonary adenocarcinoma expressing brain-specific angiogenesis inhibitor 1 (BAI1). Int J Mol Med 5: 181-183, 2000.
37. Pantaleo MA, Nicoletti G, Nanni C, *et al*: Preclinical evaluation of KIT/PDGFRA and mTOR inhibitors in gastrointestinal stromal tumors using small animal FDG PET. J Exp Clin Cancer Res 29: 173, 2010.
38. Moroz MA, Kochetkov T, Cai S, *et al*: Imaging colon cancer response following treatment with AZD1152: a preclinical analysis of [18F]fluoro-2-deoxyglucose and 3'-deoxy-3'-[18F] fluorothymidine imaging. Clin Cancer Res 17: 1099-1110, 2011.
39. Kubota K, Nakamoto Y, Tamaki N, *et al*: FDG-PET for the diagnosis of fever of unknown origin: a Japanese multi-center study. Ann Nucl Med 25: 355-364, 2011.
40. Tsukada H, Sato K, Fukumoto D, Nishiyama S, Harada N and Kakiuchi T: Evaluation of D-isomers of O-11C-methyl tyrosine and O-18F-fluoromethyl tyrosine as tumor-imaging agents in tumor-bearing mice: comparison with L- and D-11C-methionine. J Nucl Med 47: 679-688, 2006.
41. Tsukada H, Sato K, Fukumoto D and Kakiuchi T: Evaluation of D-isomers of O-18F-fluoromethyl, O-18F-fluoroethyl and O-18F-fluoropropyl tyrosine as tumour imaging agents in mice. Eur J Nucl Med Mol Imaging 33: 1017-1024, 2006.
42. Perk LR, Stigter-van Walsum M, Visser GW, *et al*: Quantitative PET imaging of Met-expressing human cancer xenografts with 89Zr-labelled monoclonal antibody DN30. Eur J Nucl Med Mol Imaging 35: 1857-1867, 2008.
43. Wang H, Liu B, Tian JH, *et al*: Monitoring early responses to irradiation with dual-tracer micro-PET in dual-tumor bearing mice. World J Gastroenterol 16: 5416-5423, 2010.

PLOS ONE

Feeder-Free Generation and Long-Term Culture of Human Induced Pluripotent Stem Cells Using Pericellular Matrix of Decidua Derived Mesenchymal Cells

Hayato Fukusumi[1], Tomoko Shofuda[2], Daisuke Kanematsu[1], Atsuyo Yamamoto[2], Hiroshi Suemizu[5], Masato Nakamura[5,6], Mami Yamasaki[3,4,9], Masatoshi Ohgushi[7], Yoshiki Sasai[8], Yonehiro Kanemura[1,4]*

1 Division of Regenerative Medicine, Institute for Clinical Research, Osaka National Hospital, National Hospital Organization, Osaka, Japan, **2** Division of Stem Cell Research, Institute for Clinical Research, Osaka National Hospital, National Hospital Organization, Osaka, Japan, **3** Division of Molecular Medicine, Institute for Clinical Research, Osaka National Hospital, National Hospital Organization, Osaka, Japan, **4** Department of Neurosurgery, Osaka National Hospital, National Hospital Organization, Osaka, Japan, **5** Biomedical Research Department, Central Institute for Experimental Animals, Kawasaki, Kanagawa, Japan, **6** Department of Pathology and Regenerative Medicine, Tokai University School of Medicine, Isehara, Kanagawa, Japan, **7** Unit for Human Stem Cell Technology, Center for Developmental Biology, RIKEN, Kobe, Hyogo, Japan, **8** Organogenesis and Neurogenesis Group, Center for Developmental Biology, RIKEN, Kobe, Hyogo, Japan, **9** Department of Pediatric Neurosurgery, Takatsuki General Hospital, Takatsuki, Osaka, Japan

Abstract

Human ES cells (hESCs) and human induced pluripotent stem cells (hiPSCs) are usually generated and maintained on living feeder cells like mouse embryonic fibroblasts or on a cell-free substrate like Matrigel. For clinical applications, a quality-controlled, xenobiotic-free culture system is required to minimize risks from contaminating animal-derived pathogens and immunogens. We previously reported that the pericellular matrix of decidua-derived mesenchymal cells (PCM-DM) is an ideal human-derived substrate on which to maintain hiPSCs/hESCs. In this study, we examined whether PCM-DM could be used for the generation and long-term stable maintenance of hiPSCs. Decidua-derived mesenchymal cells (DMCs) were reprogrammed by the retroviral transduction of four factors (OCT4, SOX2, KLF4, c-MYC) and cultured on PCM-DM. The established hiPSC clones expressed alkaline phosphatase, hESC-specific genes and cell-surface markers, and differentiated into three germ layers in vitro and in vivo. At over 20 passages, the hiPSCs cultured on PCM-DM held the same cellular properties with genome integrity as those at early passages. Global gene expression analysis showed that the GDF3, FGF4, UTF1, and XIST expression levels varied during culture, and GATA6 was highly expressed under our culture conditions; however, these gene expressions did not affect the cells' pluripotency. PCM-DM can be conveniently prepared from DMCs, which have a high proliferative potential. Our findings indicate that PCM-DM is a versatile and practical human-derived substrate that can be used for the feeder-cell-free generation and long-term stable maintenance of hiPSCs.

Citation: Fukusumi H, Shofuda T, Kanematsu D, Yamamoto A, Suemizu H, et al. (2013) Feeder-Free Generation and Long-Term Culture of Human Induced Pluripotent Stem Cells Using Pericellular Matrix of Decidua Derived Mesenchymal Cells. PLoS ONE 8(1): e55226. doi:10.1371/journal.pone.0055226

Editor: Antonio Paolo Beltrami, University of Udine, Italy

Received May 29, 2012; **Accepted** December 20, 2012; **Published** January 31, 2013

Copyright: © 2013 Fukusumi et al. This is an open-access article distributed under the terms of the Creative Commons Attribution License, which permits unrestricted use, distribution, and reproduction in any medium, provided the original author and source are credited.

Funding: This study was supported by the Project for the Realization of Regenerative Medicine from the Ministry of Education, Culture, Sports, Science and Technology (MEXT) of Japan, the Cooperative Link of Unique Science and Technology for Economy Revitalization (CLUSTER) project from MEXT, Japan, and the Research on New Drug Development, Health and Labour Sciences Research Grants, the Ministry of Health, Labour and Welfare (MHLW) of Japan. The funders had no role in study design, data collection and analysis, decision to publish, or preparation of the manuscript.

Competing Interests: The authors have declared that no competing interests exist.

* E-mail: kanemura@onh.go.jp

Introduction

Induced pluripotent stem cells (iPSCs) are generated from various somatic cells by introducing defined transcription factors [1,2], and they have properties similar to those of embryonic stem cells (ESCs). iPSCs are expected to contribute greatly not only to the realization of regenerative medicine but also to understanding the molecular pathogenesis of many currently intractable diseases. The promise of cell-based therapies using human iPSCs (hiPSCs) is generally recognized, and has driven an intense search for good cell sources, reprogramming methods, and cell culture systems. However, their clinical application has yet to be realized.

In general, hiPSCs/human ESCs (hESCs) are generated and maintained on living feeder cells, such as mouse embryonic fibroblasts (MEFs) [2–4] or SNL cells [1,5], or on a feeder-free culture substrate such as Matrigel [6–9], fibronectin [10–13], or human recombinant laminin-511 [14,15]. For clinical applications, quality-controlled xenobiotic-free culture systems are required to minimize health risks from animal-derived pathogens and immunogens [16,17]. Therefore, the use of primary human-derived living cells, like fibroblasts [18–21] or amnion-derived cells [22], is a hopeful approach, although some difficulties with these methods must still be overcome. We previously reported that the pericellular matrix of decidua-derived mesenchymal cells (PCM-DM) is an ideal human-derived material for maintaining hiPSCs/hESCs [23]. The maintenance activity of PCM-DM is similar to that of Matrigel, and its preparation is easy and reproducible, because decidua-derived mesenchymal cells (DMCs) can be obtained and expanded in large quantity [23].

In this study, we examined whether PCM-DM could be used for the feeder-free generation of hiPSCs and whether PCM-DM could maintain the cellular properties of hiPSCs over many passages.

DMCs were reprogrammed by the retroviral transduction of four factors (OCT4, SOX2, KLF4, and c-MYC; i.e., OSKM) and cultured on PCM-DM. The hiPSCs established on PCM-DM (hiPSC-PCMDM) expressed alkaline phosphatase (ALP) activity and hESC-specific genes and surface markers, and they differentiated into all three germ layers in vitro and in vivo. After over 20 passages, the cellular properties were similar to those of the cells assayed at early passages and had genomic integrity. Global gene expression analysis showed that the expression levels of GDF3, FGF4, UTF1, and XIST varied during culture and GATA6 expression was high under our conditions; the expression of these genes did not affect pluripotency. These findings suggest that PCM-DM is a practical, human-derived substrate that can be used for both the generation and stable maintenance of hiPSCs.

Materials and Methods

Human Tissue and Cells

This study was carried out in accordance with the principles of the Helsinki Declaration, and approval to use human tissues was obtained from the ethical committee of Osaka National Hospital. The donor bloods were serologically tested for HBs, HCV, HIV, and syphilis. Full-term placental tissues and results of donor blood tests were collected at the Osaka National Hospital with written informed consent.

Human ESCs (clone KhES1) were obtained from Kyoto University (Kyoto, Japan) [24] and propagated at the Center for Developmental Biology, RIKEN, in accordance with Japanese guidelines on the utilization of human ES cells, under approval from the Ministry of Education, Culture, Sports, Science and Technology (MEXT) of Japan. Human iPS cells (clone 201B7) [1] were obtained from the RIKEN cell bank (Tsukuba, Japan) and propagated on mitomycin C-treated SNL feeder cells in Primate ES cell medium (ReproCELL, Kanagawa Japan) with basic fibroblast growth factor (bFGF; 4 ng/ml; R&D Systems, Minneapolis MN) or mitomycin C-treated mouse embryonic fibroblast (MEF) feeder cells in DMEM/F-12 (1:1)-based culture medium, with 20% KnockOut SR (KSR, Invitrogen)/non-essential amino acids (0.1 mM, Invitrogen)/L-glutamine (2 mM, Invitrogen)/2-Mercaptoethanol (0.1 mM; Invitrogen)/bFGF (5 ng/ml; Wako Pure Chemical Industries, Ltd, Osaka Japan)/antibiotic-antimycotic, as previously described (hESC medium) [2,25].

Preparation of PCM-DM

Human DMCs were propagated from human term decidua vera in the DMEM/F-12 (1:1)-based culture medium supplemented with 10% fetal bovine serum (FBS), HEPES (15 mM), and antibiotic-antimycotic (Invitrogen) at 37°C in 5% CO_2 as previously described [23,26]. PCM-DM was prepared as described previously [23]. Briefly, DMCs were seeded at 3.5×10^4 cells/cm^2 on gelatin-precoated culture plates in the culture medium at 37°C in 5% CO_2. After three days in culture, the cells were rinsed with PBS once and treated with deoxycholate solution (0.5% sodium deoxycholate in 10 mM Tris-HCl, pH 8.0) at 4°C for 30 min. The treated plates were then washed six times with PBS by pipetting to flush off the cell debris, and stored under semi-dry conditions at 4°C.

Generation and Propagation of hiPSCs on PCM-DM

Four pMXs retroviral vectors encoding four reprogramming factors (OSKM) were obtained from Addgene, Inc (Cambridge, MA) [1], and amphotropic retroviruses were produced by the transfection of Platinum-A retroviral packaging cells (Cell Biolabs Inc, San Diego, CA) using FuGENE® 6 Transfection Reagent (Roche Diagnostics, Indianapolis, IN). DMCs were infected with the retrovirus supernatants supplemented with polybrene (4 μg/ml, Nacalai, Kyoto, Japan). Three days post-infection, the cells were plated on PCM-DM at 2×10^4 cells/60-mm-diameter culture dish, and the culture medium was exchanged the next day with MEF-conditioned medium (MEF-CM), prepared as described previously [6]. Briefly, mitomycin C-treated MEF cells were cultured on gelatin-coated plates in hESC medium consisting of DMEM/F-12 (1:1)-based culture medium with 20% KnockOut SR (KSR, Invitrogen)/non-essential amino acids (0.1 mM, Invitrogen)/L-glutamine (2 mM, Invitrogen)/2-Mercaptoethanol (0.1 mM; Invitrogen)/bFGF (5 ng/ml; Wako Pure Chemical Industries, Ltd, Osaka Japan)/antibiotic-antimycotic for 24 hours at 37°C in 5% CO_2. The supernatant was then collected and supplemented with an additional 5 ng/ml bFGF. The medium was changed daily until hESC-like colonies appeared. After 30 days of induction, the hESC-like colonies were picked up and replated on PCM-DM in MEF-CM (passage 1). After passage 2, the established hiPSCs were cultured with STEM-PRO hESC SFM (StemPro, Invitrogen) on PCM-DM (Fig. 1A).

Human iPSCs (201B7) propagated on SNL feeder cells in hESC medium were also cultured on PCM-DM in MEF-CM or StemPro medium.

Cell Reprogramming Efficiency Using PCM-DM Versus Other Substrates

Six different DMC lines (DMC71, DMC72, DMC75, DMC76, DMC85 and DMC92) were reprogrammed under seven different culture conditions (6×10^4 cells per culture), as follows: plated on MEFs with non-conditioned (NC)-hESC medium (control), on PCM-DM with MEF-CM, on Matrigel with MEF-CM, on gelatin with MEF-CM (autologous feeder) [27], on PCM-DM with NC-hESC medium, on Matrigel with NC-hESC medium, and on gelatin with NC-hESC medium. Cells reprogrammed using PCM-DM with NC-hESC medium were propagated further for detailed analyses.

ALP Staining

Cells were fixed with 10% Formalin/PBS for 2 min. The fixed cells were washed with PBS once and then stained with 1-Step NBT/BCIP (Thermo SCIENTIFIC, Rockford, IL) for 30 min at room temperature (RT), according to the manufacturer's specification.

Quantitative Reverse Transcription-polymerase Chain Reaction (qRT-PCR)

Total RNA was extracted as described in the RNeasy Mini Kit (Qiagen, Valencia, CA), and cDNA was synthesized from 1 μg total RNA using random hexamers for reverse transcription, according to the manufacturer's specification (SuperScript First-Strand Synthesis System for RT-PCR, Invitrogen). Quantitative PCR analysis was performed using gene-specific primers (Supplemental Table S1) with Power SYBR® Green PCR Master Mix, the 7300 real-time PCR system (Applied Biosystems, Foster, CA), and the comparative Ct method or standard curve method [28].

Flow Cytometry (FCM) Analysis

Cells were pre-incubated with Y-27632 (Wako Pure Chemical Industries) for 30 min and then dissociated by trypsin/EDTA (Invitrogen). The dissociated cells were fixed with 4% paraformaldehyde (PFA) for 20 min on ice, washed with PBS, and then reacted with the following primary antibodies for 30 min at 4°C: